

10078  
P-38

# Combined Compressive and Shear Buckling Analysis of Hypersonic Aircraft Structural Sandwich Panels

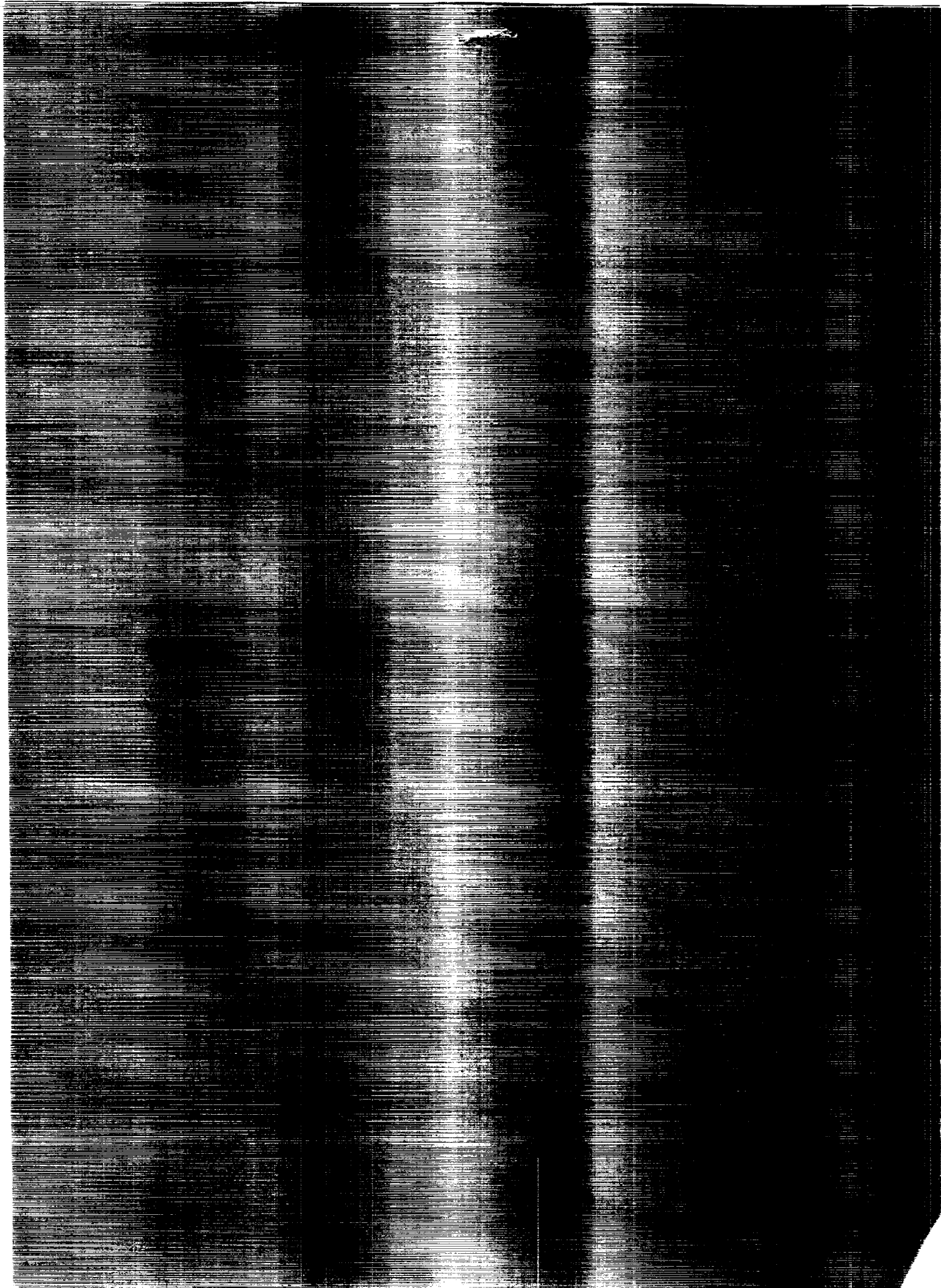
William L. Ko and Raymond H. Jones

MAY 1991

COMBINED COMPRESSIVE AND SHEAR BUCKLING ANALYSIS OF  
HYPERSONIC AIRCRAFT STRUCTURAL SANDWICH PANELS (NASA)  
58-5

CSCL 20K

41/59 unclas  
0019928



NASA Technical Memorandum 4290

# Combined Compressive and Shear Buckling Analysis of Hypersonic Aircraft Structural Sandwich Panels

William L. Ko and Raymond H. Jackson  
*Ames Research Center*  
*Dryden Flight Research Facility*  
*Edwards, California*



National Aeronautics and  
Space Administration  
Office of Management  
Scientific and Technical  
Information Division

1991

Dr. William L. Ko and the Dryden Flight Research Facility community would like to acknowledge the hard work and dedication of Raymond H. Jackson, whose recent death occurred during the final stages of this report. He and Dr. Ko were also completing several other reports prior to his death. Mr. Jackson contributed greatly to the programming of complicated mathematical equations for studying buckling behavior of structural panels for the National AeroSpace Plane.

**CONTENTS**

<b>1</b>	<b>ABSTRACT</b>	<b>1</b>
<b>2</b>	<b>INTRODUCTION</b>	<b>1</b>
<b>3</b>	<b>NOMENCLATURE</b>	<b>1</b>
<b>4</b>	<b>HOT STRUCTURAL PANELS</b>	<b>3</b>
<b>5</b>	<b>BUCKLING ANALYSIS</b>	<b>5</b>
5.1	Panel Constitutive Equations . . . . .	5
5.2	Panel Boundary Conditions . . . . .	6
5.3	Energy Equations . . . . .	6
5.4	Rayleigh-Ritz Method . . . . .	7
<b>6</b>	<b>NUMERICAL RESULTS</b>	<b>10</b>
6.1	Physical Properties of Panels . . . . .	10
6.2	Convergency of Eigenvalue Solutions . . . . .	12
6.3	Buckling Interaction Curves . . . . .	14
<b>7</b>	<b>CONCLUDING REMARKS</b>	<b>28</b>
	<b>APPENDIX —FLEXURAL, TWISTING, AND TRANVERSE SHEAR STIFFNESSES</b>	<b>29</b>
	<b>REFERENCES</b>	<b>32</b>



## 1 ABSTRACT

The combined-load (compression and shear) buckling equations were established for orthotropic sandwich panels by using the Rayleigh-Ritz method to minimize the panel total potential energy. The resulting combined-load buckling equations were used to generate buckling interaction curves for super-plastically-formed/ diffusion-bonded titanium truss-core sandwich panels and titanium honeycomb-core sandwich panels having the same specific weight. The relative combined-load buckling strengths of these two types of sandwich panels are compared with consideration of their sandwich core orientations. For square and nearly square panels of both types, the combined load always induces symmetric buckling. As the panel aspect ratios increase, antisymmetric buckling will show up when the loading is shear-dominated combined loading. The square panel (either type) has the highest combined buckling strength, but the combined load buckling strength drops sharply as the panel aspect ratio increases. For square panels, the truss-core sandwich panel has higher compression-dominated combined-load buckling strength. However, for shear dominated loading, the square honeycomb-core sandwich panel has higher shear-dominated combined load buckling strength.

## 2 INTRODUCTION

Extensive explorative work has been carried out to find highly efficient (high stiffness, low specific weight) hot structural panel concepts for application to hypersonic flight vehicles such as the National AeroSpace Plane (NASP, refs. 1–12). The typical high-efficiency hot structural panels investigated hitherto are tubular and beaded panels (refs. 1–11) made of René 41, and sandwich panels with different core geometries, fabricated with superalloys (e.g., titanium, Inconel 617<sup>®</sup>, René 41). The face sheets of the sandwich panel may be either continuous alloy or metal-matrix composites (e.g., silicon carbide/titanium metal-matrix composites, ref. 12).

During applications (or services), the hot structural panel will be subjected to combined loading induced by aerodynamic and thermal loadings. Therefore, the critical requirement for those hot structural panels is the high buckling strength. The buckling behavior of tubular and beaded panels has been studied extensively theoretically and experimentally (refs. 9–11). References 13 and 14 report some results of the compressive buckling behavior of truss-core and honeycomb-core sandwich panels.

Because these two types of sandwich panels could be good candidates for applications to the NASP, it is important to understand the relative structural performances of those two panels under the combined loadings. This report compares the buckling strengths of the truss-core and honeycomb-core sandwich panels of identical specific weight subjected to combined compressive and shear loadings.

## 3 NOMENCLATURE

$A_{mn}$	Fourier coefficient of trial function for $w$ , in
$a$	length of sandwich panel, in
$a_{mn}^{ij}$	coefficients of characteristic equations
$B_{mn}$	Fourier coefficient of trial function for $\gamma_x$ , rad
$b$	horizontal projected length of corrugation leg excluding the flat segments, in
$C_{mn}$	Fourier coefficient of trial function for $\gamma_y$ , rad
$c$	width of sandwich panel, in

---

<sup>®</sup>Inconel is a registered trademark of Huntington Alloy Products Division, International Nickel Company, Huntington, WV.

$D^*$	flexural stiffness parameter, $\sqrt{\bar{D}_x \bar{D}_y}$ , in-lb
$D_{Qx}, D_{Qy}$	transverse shear stiffnesses in planes parallel and normal to the corrugation axis ( $x$ -axis), lb/in-rad
$D_x, D_y$	longitudinal and transverse panel flexural stiffnesses, in-lb
$\bar{D}_x, \bar{D}_y$	panel flexural stiffnesses, in-lb
$D_{xy}$	panel twisting stiffness, in-lb
$D_z^F, D_y^H, D_z^H$	nondimensional parameters that are functions of truss-core geometric parameters
$d$	one half the length of straight diagonal segment of corrugation leg, in
$E_c$	Young's modulus of sandwich core material, lb/in <sup>2</sup>
$E_{cx}, E_{cy}, E_{cz}$	effective Young's moduli of honeycomb core, lb/in <sup>2</sup>
$E_x, E_y$	Young's moduli of face sheets, lb/in <sup>2</sup>
$f$	length of flat horizontal region of corrugation leg, in
$G_c$	shear modulus of sandwich core material, lb/in <sup>2</sup>
$G_{cxy}, G_{cyz}, G_{czx}$	effective shear moduli of honeycomb core, lb/in <sup>2</sup>
$G_{xy}$	shear modulus of face sheets, lb/in <sup>2</sup>
$h$	depth of sandwich panel = distance between middle planes of two face sheets, in
$h_c$	depth of corrugation = vertical distance between center lines of upper and lower flat segments of corrugation leg, $h_c = h - t_s - t_f$ , in
$h'_c$	depth of honeycomb core, $h'_c = h - t_s$ , in
$I_c$	moment of inertia, per unit width, of truss-core sheet of thickness $t_c$ , $I_c = \frac{1}{12} t_c^3$ , in <sup>4</sup> /in
$\bar{I}_c$	moment of inertia, per unit width, of truss-core cross section taken with respect to the horizontal centroidal axis of the corrugation cross section, in <sup>4</sup> /in
$I_f$	moment of inertia, per unit width, of corrugation leg flat region of thickness $t_f$ , $I_f = \frac{1}{12} t_f^3$ , in <sup>4</sup> /in
$I_s$	moment of inertia, per unit width, of two face sheets, taken with respect to horizontal centroidal axis (neutral axis) of the sandwich panel, $I_s = \frac{1}{2} t_s h^2 + \frac{1}{6} t_s^3$ , in <sup>4</sup> /in
$i$	index, 1,2,3, ...
$j$	index, 1,2,3, ...
$k_x$	compressive buckling load factor, $k_x = \frac{N_x a^2}{\pi^2 D^*}$
$k_{xy}$	shear buckling load factor, $k_{xy} = \frac{N_{xy} a^2}{\pi^2 D^*}$
$\ell$	length of corrugation leg, in
$M_x, M_y$	bending moment intensities, in-lb/in
$M_{xy}$	twisting moment intensities, in-lb/in



$m$	number of buckle half waves in $x$ -direction
$N_x, N_y$	normal stress resultants, lb/in
$N_{xy}$	shear stress resultant, lb/in
$n$	number of buckle half waves in $y$ -direction
$p$	one half of corrugation pitch = half wave length of corrugation, in
$Q_x, Q_y$	transverse shear force intensities, lb/in
$R$	radius of circular arc regions of corrugation leg, in
$R_x$	compressive stress ratio, $R_x = \frac{k_x}{k_x(\text{pure compression})}$
$R_{xy}$	shear stress ratio, $R_{xy} = \frac{k_{xy}}{k_{xy}(\text{pure shear})}$
$\bar{S}$	transverse shear stiffness parameter
$t_c$	thickness of straight diagonal segment, or circular arc regions of corrugation leg, $t_c = t_f \frac{p-f}{\ell-f}$ , in
$t_f$	thickness of corrugation leg horizontal flat segments, in
$t_s$	thickness of sandwich face sheets, in
$V$	total potential energy of sandwich panel, in-lb
$V_1$	strain energy of the sandwich panel, in-lb
$V_2$	work done by external loads, in-lb
$w$	panel deflection, in
$x, y, z$	rectangular Cartesian coordinates
$\gamma_x, \gamma_y$	thickness shear strains, rad
$\delta_{mnij}$	special delta function obeying $m \neq i, n \neq j$ , $m \pm i = \text{odd}, n \pm j = \text{odd}, \delta_{mnij} = \frac{mnij}{(m^2 - i^2)(n^2 - j^2)}$
$\theta$	corrugation angle, rad
$\nu_c$	Poisson ratio of sandwich core material
$\nu_{cxy}, \nu_{cyz}, \nu_{cxz}$	Poisson ratios of honeycomb core
$\nu_{xy}, \nu_{yx}$	Poisson ratios of face sheets, also for sandwich panel
$\rho_{HC}$	specific weight of honeycomb core, lb/in <sup>3</sup>
$\rho_{Ti}$	specific weight of titanium material, lb/in <sup>3</sup>

## 4 HOT STRUCTURAL PANELS

Figures 1 and 2 show titanium truss-core and honeycomb-core sandwich panels, respectively. The truss-core sandwich panel may be fabricated by a superplastic-forming/diffusion-bonding process. The honeycomb-core sandwich panel can be fabricated by an enhanced-diffusion bonding process which joins the two face sheets to the

honeycomb core (ref. 12). To compare the buckling strength, both types of the sandwich panels have the same face sheet thickness and same core depth. The thickness of the truss is adjusted so that the two types of panels will have identical specific weight. The sandwich panels will be subjected to combined compressive and shear loadings as shown in figure 3. For each type of panel, two cases of core orientations will be investigated. Namely, truss-core orientation,

- case 1 = corrugation axis parallel to  $N_x$  and
- case 2 = corrugation axis perpendicular to  $N_x$ ;

honeycomb-core orientation,

- case 1 = hexagon longitudinal axis parallel to  $N_x$  and
- case 2 = hexagon longitudinal axis perpendicular to  $N_x$ .

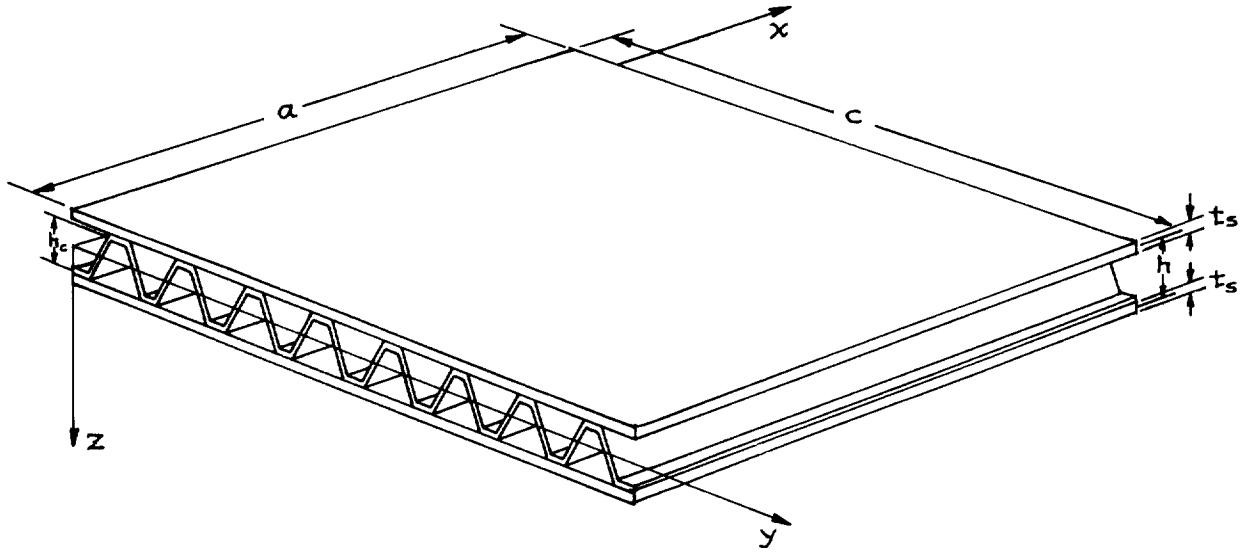


Figure 1. Truss-core sandwich panel.

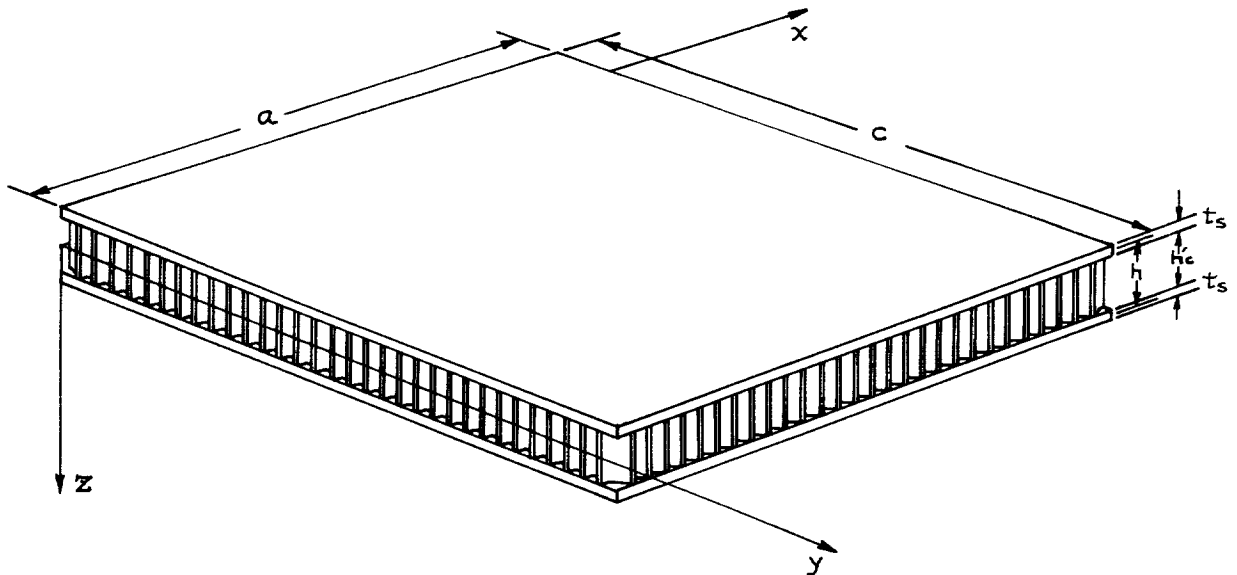


Figure 2. Honeycomb-core sandwich panel.

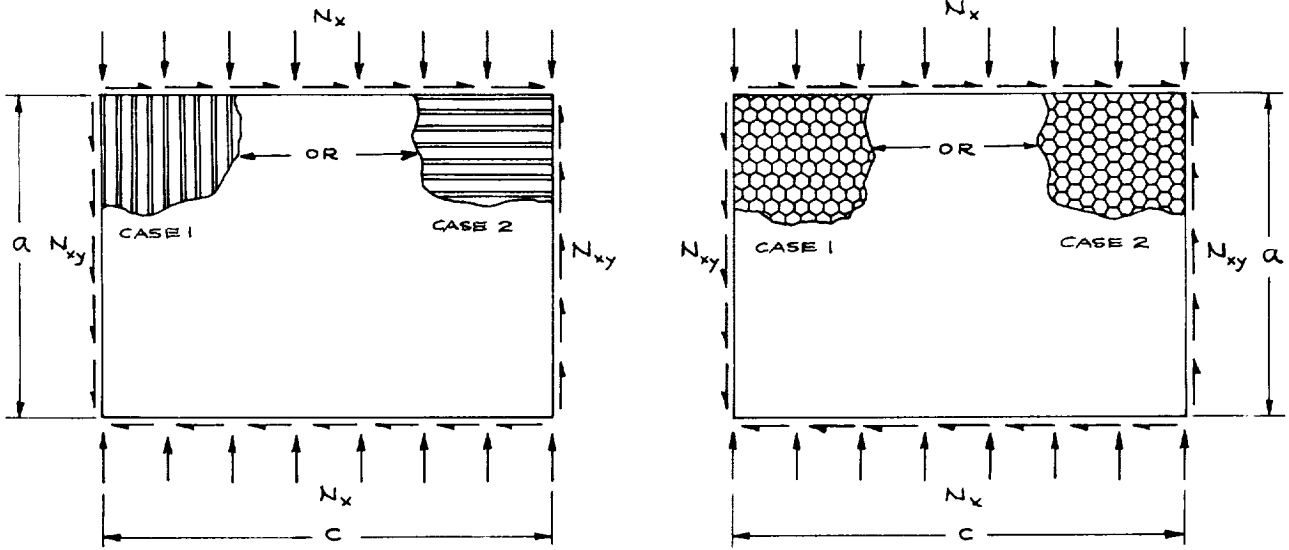


Figure 3. Truss-core and honeycomb-core sandwich panels of the same specific weight under compression and shear.

## 5 BUCKLING ANALYSIS

### 5.1 Panel Constitutive Equations

The sandwich panel constitutive equations (moment and shear equations, ref. 15) may be expressed as

$$M_x = -\frac{D_x}{1 - \nu_{xy}\nu_{yx}} \left[ \frac{\partial}{\partial x} \left( \frac{\partial w}{\partial x} - \gamma_x \right) + \nu_{yx} \frac{\partial}{\partial y} \left( \frac{\partial w}{\partial y} - \gamma_y \right) \right] \quad (1)$$

$$M_y = -\frac{D_y}{1 - \nu_{xy}\nu_{yx}} \left[ \frac{\partial}{\partial y} \left( \frac{\partial w}{\partial y} - \gamma_y \right) + \nu_{xy} \frac{\partial}{\partial x} \left( \frac{\partial w}{\partial x} - \gamma_x \right) \right] \quad (2)$$

$$M_{xy} = \frac{D_{xy}}{2} \left[ \frac{\partial}{\partial x} \left( \frac{\partial w}{\partial y} - \gamma_y \right) + \frac{\partial}{\partial y} \left( \frac{\partial w}{\partial x} - \gamma_x \right) \right] \quad (3)$$

$$Q_x = D_{Qx} \gamma_x \quad (4)$$

$$Q_y = D_{Qy} \gamma_y \quad (5)$$

where  $M_x$  and  $M_y$  are the bending moment intensities,  $M_{xy}$  is the twisting moment intensity,  $Q_x$  and  $Q_y$  are the intensities of transverse shear resultants (fig. 4),  $w$  is the panel deflection,  $\gamma_x$  and  $\gamma_y$  are the transverse shear strains,  $\nu_{xy}$  and  $\nu_{yx}$  are the panel Poisson ratios,  $D_x$  and  $D_y$  are the flexural stiffnesses,  $D_{xy}$  is the twisting stiffness, and  $D_{Qx}$  and  $D_{Qy}$  are the transverse shear stiffnesses.  $D_x$ ,  $D_y$ ,  $D_{xy}$ ,  $D_{Qx}$ , and  $D_{Qy}$  are defined in the appendix.

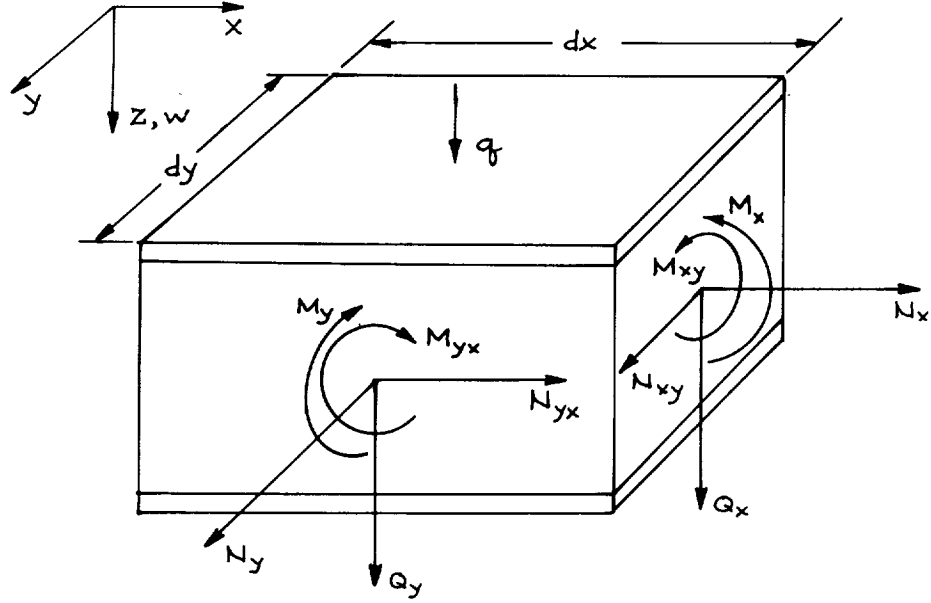


Figure 4. Forces and moments acting on a differential element of a sandwich panel.

## 5.2 Panel Boundary Conditions

The sandwich panels will be assumed to be simply supported at four edges. Namely

$$w = M_x = \gamma_y = 0 \quad \text{along} \quad x = 0, a \quad (6)$$

$$w = M_y = \gamma_x = 0 \quad \text{along} \quad y = 0, c \quad (7)$$

## 5.3 Energy Equations

The strain energy  $V_1$  produced by the moments  $M_x$ ,  $M_y$ ,  $M_{xy}$  ( $= M_{yx}$ ), and the transverse shear forces  $Q_x$  and  $Q_y$  (fig. 4) may be written as (ref. 15)

$$\begin{aligned} V_1 = \frac{1}{2} \int_0^a \int_0^c \left\{ \frac{D_x}{1 - \nu_{xy}\nu_{yx}} \left[ \frac{\partial}{\partial x} \left( \frac{\partial w}{\partial x} - \gamma_x \right) \right]^2 \right. \\ + \frac{D_x \nu_{yx} + D_y \nu_{xy}}{1 - \nu_{xy}\nu_{yx}} \left[ \frac{\partial}{\partial x} \left( \frac{\partial w}{\partial x} - \gamma_x \right) \right] \left[ \frac{\partial}{\partial y} \left( \frac{\partial w}{\partial y} - \gamma_y \right) \right] \\ \times \frac{D_y}{1 - \nu_{xy}\nu_{yx}} \left[ \frac{\partial}{\partial y} \left( \frac{\partial w}{\partial y} - \gamma_y \right) \right]^2 + \frac{D_{xy}}{2} \left[ \frac{\partial}{\partial x} \left( \frac{\partial w}{\partial y} - \gamma_y \right) + \frac{\partial}{\partial y} \left( \frac{\partial w}{\partial x} - \gamma_x \right) \right]^2 \\ \left. + D_{Qx} \gamma_x^2 + D_{Qy} \gamma_y^2 \right\} dx dy \quad (8) \end{aligned}$$

and the strain energy  $V_2$  produced by the external loads  $N_x$ ,  $N_y$ ,  $N_{xy}$ , and  $q$  can be expressed as (ref. 15)

$$V_2 = \frac{1}{2} \int_0^a \int_0^c \left[ -2qw + N_x \left( \frac{\partial w}{\partial x} \right)^2 + N_y \left( \frac{\partial w}{\partial y} \right)^2 + 2N_{xy} \frac{\partial w}{\partial x} \frac{\partial w}{\partial y} \right] dx dy \quad (9)$$

Then, the total potential energy  $V$  of the sandwich system is given

$$V = V_1 + V_2 \quad (10)$$

For the present problem,  $q = N_y = 0$ , and  $N_x \rightarrow -N_x$ .

#### 5.4 Rayleigh-Ritz Method

Because of the existence of the shear loading term  $N_{xy} \frac{\partial w}{\partial x} \frac{\partial w}{\partial y}$  appearing in equation (9), the Rayleigh-Ritz method will be used to minimize the total potential energy  $V$  of the sandwich system to obtain the buckling equation for combined loading.

To satisfy the simply-supported boundary conditions equations (6) and (7), the following trial functions for the panel deflection  $w$  and the transverse shear strains  $\gamma_x$  and  $\gamma_y$  may be chosen (ref. 16)

$$w = \sum_{m=1}^{\infty} \sum_{n=1}^{\infty} A_{mn} \sin \frac{m\pi x}{a} \sin \frac{n\pi y}{c} \quad (11)$$

$$\gamma_x = \sum_{m=1}^{\infty} \sum_{n=1}^{\infty} B_{mn} \cos \frac{m\pi x}{a} \sin \frac{n\pi y}{c} \quad (12)$$

$$\gamma_y = \sum_{m=1}^{\infty} \sum_{n=1}^{\infty} C_{mn} \sin \frac{m\pi x}{a} \cos \frac{n\pi y}{c} \quad (13)$$

where  $A_{mn}$ ,  $B_{mn}$ , and  $C_{mn}$  are the undetermined Fourier coefficients of the assumed trial functions for  $w$ ,  $\gamma_x$ , and  $\gamma_y$  respectively, and  $m$  and  $n$  are the buckle half wave numbers in the  $x$  and  $y$  direction. Substitution of equations (11) through (13) into equations (8) and (9) and then substitution of the resulting expressions of  $V_1$  and  $V_2$  into equation (10), and applying the Rayleigh principle of minimizing  $V$

$$\frac{\partial V}{\partial A_{mn}} = \frac{\partial V}{\partial B_{mn}} = \frac{\partial V}{\partial C_{mn}} = 0 \quad (14)$$

one obtains three simultaneous characteristic equations for the determination of the combined buckling loads.

For  $\frac{\partial V}{\partial A_{mn}} = 0$

$$\left( a_{mn}^{11} - k_x \frac{m^2 \pi^4}{a^4} \right) A_{mn} + 32 \frac{\pi^2 k_{xy}}{a^3 c} \sum_{i=1}^{\infty} \sum_{j=1}^{\infty} \delta_{mni j} A_{ij} + a_{mn}^{12} B_{mn} + a_{mn}^{13} C_{mn} = 0 \quad (15)$$

For  $\frac{\partial V}{\partial B_{mn}} = 0$

$$a_{mn}^{21} A_{mn} + a_{mn}^{22} B_{mn} + a_{mn}^{23} C_{mn} = 0 \quad (16)$$

For  $\frac{\partial V}{\partial C_{mn}} = 0$

$$a_{mn}^{31} A_{mn} + a_{mn}^{32} B_{mn} + a_{mn}^{33} C_{mn} = 0 \quad (17)$$

In equation (15), the buckling load factors  $k_x$  and  $k_{xy}$  are respectively defined as

$$k_x = \frac{N_x a^2}{\pi^2 D^*}, \quad k_{xy} = \frac{N_{xy} a^2}{\pi^2 D^*} \quad (18)$$

where the flexural stiffness parameter  $D^*$  is defined as

$$D^* = \frac{\sqrt{E_x E_y}}{1 - \nu_{xy} \nu_{yx}} I_s \quad (19)$$

In addition, the special delta function  $\delta_{mnij}$  appearing in equation (15) is defined as

$$\delta_{mnij} = \frac{mni j}{(m^2 - i^2)(n^2 - j^2)} \quad (20)$$

which obeys the conditions:  $m \neq i, n \neq j, m \pm i = \text{odd}, n \pm j = \text{odd}$ .

The coefficients  $a_{mn}^{ij}$  ( $i, j = 1, 2, 3$ ) appearing in equations (15) through (17) are defined as follows

$$a_{mn}^{11} = \bar{D}_x \left( \frac{m\pi}{a} \right)^4 + (\bar{D}_x \nu_{yx} + \bar{D}_y \nu_{xy} + 2 D_{xy}) \left( \frac{m\pi}{a} \right)^2 \left( \frac{n\pi}{c} \right)^2 + \bar{D}_y \left( \frac{n\pi}{c} \right)^4 \quad (21)$$

$$a_{mn}^{12} = a_{mn}^{21} = - \left[ \bar{D}_x \left( \frac{m\pi}{a} \right)^3 + \frac{1}{2} (\bar{D}_x \nu_{yx} + \bar{D}_y \nu_{xy} + 2 D_{xy}) \left( \frac{m\pi}{a} \right) \left( \frac{n\pi}{c} \right)^2 \right] \quad (22)$$

$$a_{mn}^{13} = a_{mn}^{31} = - \left[ \bar{D}_y \left( \frac{n\pi}{c} \right)^3 + \frac{1}{2} (\bar{D}_x \nu_{yx} + \bar{D}_y \nu_{xy} + 2 D_{xy}) \left( \frac{m\pi}{a} \right)^2 \left( \frac{n\pi}{c} \right) \right] \quad (23)$$

$$a_{mn}^{22} = \bar{D}_x \left( \frac{m\pi}{a} \right)^2 + \frac{D_{xy}}{2} \left( \frac{n\pi}{c} \right)^2 + D_{Qx} \quad (24)$$

$$a_{mn}^{23} = a_{mn}^{32} = \frac{1}{2} (\bar{D}_x \nu_{yx} + \bar{D}_y \nu_{xy} + D_{xy}) \left( \frac{m\pi}{a} \right) \left( \frac{n\pi}{c} \right) \quad (25)$$

$$a_{mn}^{33} = \bar{D}_y \left( \frac{n\pi}{c} \right)^2 + \frac{D_{xy}}{2} \left( \frac{m\pi}{a} \right)^2 + D_{Qy} \quad (26)$$

In the previous

$$\bar{D}_x = \frac{D_x}{1 - \nu_{xy}\nu_{yx}}, \quad \bar{D}_y = \frac{D_y}{1 - \nu_{xy}\nu_{yx}} \quad (27)$$

Solving for  $B_{mn}$  and  $C_{mn}$  in terms of  $A_{mn}$  from equations (16) and (17), one obtains

$$B_{mn} = \frac{a_{mn}^{23} a_{mn}^{31} - a_{mn}^{21} a_{mn}^{33}}{a_{mn}^{22} a_{mn}^{33} - a_{mn}^{23} a_{mn}^{32}} A_{mn} \quad (28)$$

$$C_{mn} = \frac{a_{mn}^{21} a_{mn}^{32} - a_{mn}^{22} a_{mn}^{31}}{a_{mn}^{22} a_{mn}^{33} - a_{mn}^{23} a_{mn}^{32}} A_{mn} \quad (29)$$

Substitution of equations (28) and (29) into equation (15) yields a homogenous linear equation containing only the panel deflection coefficient  $A_{mn}$

$$\frac{M_{mn}}{k_{xy}} A_{mn} + \sum_{i=1}^{\infty} \sum_{j=1}^{\infty} \delta_{mnij} A_{ij} = 0 \quad (30)$$

where  $m \neq i, n \neq j, m \pm i = \text{odd}, n \pm i = \text{odd}$ , and

$$M_{mn} = \frac{ac}{32} \left\{ k_x \left( \frac{m\pi}{a} \right)^2 - \frac{a^2}{\pi^2 D^*} \left[ \underbrace{a_{mn}^{11}}_{\substack{\text{classical thin} \\ \text{plate theory term}}} + \underbrace{\frac{a_{mn}^{12} (a_{mn}^{23} a_{mn}^{31} - a_{mn}^{21} a_{mn}^{33}) + a_{mn}^{13} (a_{mn}^{21} a_{mn}^{32} - a_{mn}^{22} a_{mn}^{31})}{a_{mn}^{22} a_{mn}^{33} - a_{mn}^{23} a_{mn}^{32}}}}_{\text{transverse shear effect terms}} \right] \right\} \quad (31)$$

Equation (30) forms a system of an infinite number of simultaneous equations associated with different values of  $m$  and  $n$ . For practical purposes, the number of these simultaneous equations may be cut off up to certain finite numbers if the convergency of the eigenvalue solutions reached the desired limit. Since  $m \pm n = \text{odd}$  and  $n \pm j = \text{odd}$  is required in equation (20), we have  $(m \pm i) \pm (n \pm j) = (m \pm n) \pm (i \pm j) = \text{even}$ . Thus, if  $m \pm n = \text{even}$ , then  $(i \pm j)$  must also be even. Likewise, if  $m \pm n = \text{odd}$ , then  $(i \pm j)$  must also be odd. Therefore, there is no coupling between even case and odd case in each equation written out from equation (30) for a particular set of  $\{m, n\}$ . Namely, if the  $A_{mn}$  term in equation (30) is for  $m \pm n = \text{even}$  (or odd), then the  $A_{ij}$  term in the same equation must be for  $(i \pm j) = \text{even}$  (or odd) also. Thus, the simultaneous equations generated from equation (30) may be divided into two groups which are independent of each other; one group in which  $m \pm n$  is even (i.e., symmetrical buckling), and the other in which  $m \pm n$  is odd (i.e., antisymmetrical buckling, refs. 17, 18). For the deflection coefficients  $A_{mn}$  to have nontrivial solutions for given values of  $k_x$  and  $\frac{C}{a}$ , the determinant of the coefficients of the unknown  $A_{mn}$  must vanish. The largest eigenvalue  $\frac{1}{k_{xy}}$  thus obtained will give the lowest buckling load factor  $k_{xy}$  as a function of  $k_x$  and  $\frac{C}{a}$ . Thus, a family of buckling interaction curves in the  $k_x$ - $k_{xy}$  space may be generated with  $\frac{C}{a}$  as a parameter. Representative characteristic equations (buckling equations) for  $12 \times 12$  matrices written out from equation (30) are shown respectively in equations (32) and (33) for the cases  $m \pm n = \text{even}$  and  $m \pm n = \text{odd}$  (refs. 17, 18).

$m \pm n = \text{even}$

	$A_{11}$	$A_{13}$	$A_{22}$	$A_{31}$	$A_{15}$	$A_{24}$	$A_{33}$	$A_{42}$	$A_{51}$	$A_{35}$	$A_{44}$	$A_{53}$	
$m=1, n=1$	$\frac{M_{11}}{k_{xy}}$	0	$\frac{4}{9}$	0	0	$\frac{8}{45}$	0	$\frac{8}{45}$	0	0	$\frac{16}{225}$	0	= 0
$m=1, n=3$		$\frac{M_{13}}{k_{xy}}$	$-\frac{4}{5}$	0	0	$\frac{8}{7}$	0	$-\frac{8}{25}$	0	0	$\frac{16}{35}$	0	
$m=2, n=2$			$\frac{M_{22}}{k_{xy}}$	$-\frac{4}{5}$	$-\frac{20}{63}$	0	$\frac{36}{25}$	0	$-\frac{20}{63}$	$\frac{4}{7}$	0	$\frac{4}{7}$	
$m=3, n=1$				$\frac{M_{31}}{k_{xy}}$	0	$-\frac{8}{25}$	0	$\frac{8}{7}$	0	0	$\frac{16}{35}$	0	
$m=1, n=5$					$\frac{M_{15}}{k_{xy}}$	$-\frac{40}{27}$	0	$-\frac{8}{63}$	0	0	$-\frac{16}{27}$	0	
$m=2, n=4$						$\frac{M_{24}}{k_{xy}}$	$-\frac{72}{35}$	0	$-\frac{8}{63}$	$\frac{8}{3}$	0	$-\frac{120}{147}$	
$m=3, n=3$			Symmetry				$\frac{M_{33}}{k_{xy}}$	$-\frac{72}{35}$	0	0	$\frac{144}{49}$	0	
$m=4, n=2$								$\frac{M_{42}}{k_{xy}}$	$-\frac{40}{27}$	$-\frac{120}{147}$	0	$\frac{8}{3}$	
$m=5, n=1$									$\frac{M_{51}}{k_{xy}}$	0	$-\frac{16}{27}$	0	
$m=3, n=5$										$\frac{M_{35}}{k_{xy}}$	$-\frac{80}{21}$	0	
$m=4, n=4$											$\frac{M_{44}}{k_{xy}}$	$-\frac{80}{21}$	
$m=5, n=3$												$\frac{M_{53}}{k_{xy}}$	

(32)

where the nonzero off-diagonal terms satisfy the conditions:  $m \neq i, n \neq j, m \pm i = \text{odd}$  and  $n \pm j = \text{odd}$ .

$m \pm n = \text{odd}$

	$A_{12}$	$A_{21}$	$A_{14}$	$A_{23}$	$A_{32}$	$A_{41}$	$A_{16}$	$A_{25}$	$A_{34}$	$A_{43}$	$A_{52}$	$A_{61}$	
$m=1, n=2$	$\frac{M_{12}}{k_{xy}}$	$-\frac{4}{9}$	0	$\frac{4}{5}$	0	$-\frac{8}{45}$	0	$\frac{20}{63}$	0	$\frac{8}{25}$	0	$-\frac{4}{35}$	= 0
$m=2, n=1$		$\frac{M_{21}}{k_{xy}}$	$-\frac{8}{45}$	0	$\frac{4}{5}$	0	$-\frac{4}{35}$	0	$\frac{8}{25}$	0	$\frac{20}{63}$	0	
$m=1, n=4$			$\frac{M_{14}}{k_{xy}}$	$-\frac{8}{7}$	0	$-\frac{16}{225}$	0	$\frac{40}{27}$	0	$-\frac{16}{35}$	0	$-\frac{8}{175}$	
$m=2, n=3$				$\frac{M_{23}}{k_{xy}}$	$-\frac{36}{25}$	0	$-\frac{4}{9}$	0	$\frac{72}{35}$	0	$-\frac{4}{7}$	0	
$m=3, n=2$					$\frac{M_{32}}{k_{xy}}$	$-\frac{8}{7}$	0	$-\frac{4}{7}$	0	$\frac{72}{35}$	0	$-\frac{4}{9}$	
$m=4, n=1$						$\frac{M_{41}}{k_{xy}}$	$-\frac{8}{175}$	0	$-\frac{16}{35}$	0	$\frac{40}{27}$	0	
$m=1, n=6$			Symmetry				$\frac{M_{16}}{k_{xy}}$	$-\frac{20}{11}$	0	$-\frac{8}{45}$	0	$-\frac{36}{1225}$	
$m=2, n=5$								$\frac{M_{25}}{k_{xy}}$	$-\frac{8}{3}$	0	$-\frac{100}{441}$	0	
$m=3, n=4$									$\frac{M_{34}}{k_{xy}}$	$-\frac{144}{49}$	0	$-\frac{8}{45}$	
$m=4, n=3$										$\frac{M_{43}}{k_{xy}}$	$-\frac{8}{3}$	0	
$m=5, n=2$											$\frac{M_{52}}{k_{xy}}$	$-\frac{20}{11}$	
$m=6, n=1$												$\frac{M_{61}}{k_{xy}}$	

(33)

where the nonzero off-diagonal terms satisfy the conditions:  $m \neq i$ ,  $n \neq j$ ,  $m \pm i = \text{odd}$  and  $n \pm j = \text{odd}$ .

Notice that the diagonal terms in the determinants (eq. (32), (33)) come from the first term of equation (30), and the second series term of equation (30) gives the off-diagonal terms of the determinants.

## 6 NUMERICAL RESULTS

### 6.1 Physical Properties of Panels

The titanium truss-core and titanium honeycomb-core sandwich panels analyzed have the following geometrical and material properties.



## Geometry:

Items	Truss-core sandwich panel	Honeycomb-core sandwich panel
$a$ , in	24	24
$b = \frac{1}{2}(p - f)$ , in	0.3294	---
$\frac{c}{a}$	1, 2, 3, 4	1, 2, 3, 4
$d = \frac{b}{\cos \theta}$ , in	0.6589	---
$f$ , in	0	---
$h$ , in	1.2	1.2
$h_c = h - t_s - t_f$ , in	1.1412	---
$h'_c = h - t_s$ , in	---	1.1680
$\ell = f + 2(d + R\theta)$ , in	1.3177	---
$p = \frac{h_c}{\tan \theta}$ , in	0.6589	---
$R$ , in	0	---
$t_c = t_f \cos \theta$ , in	0.0134	---
$t_f$ , in	0.0268	---
$t_s$ , in	0.0320	0.0320
$\theta$ , deg	60	---

## Material properties

The titanium material used for the sandwich panel face sheets and cores has the following properties

$$E_x = E_y = E_c = 16 \times 10^6 \text{ lb/in}^2$$

$$G_{xy} = G_c = 6.2 \times 10^6 \text{ lb/in}^2$$

$$\nu_{xy} = \nu_{yx} = \nu_c = 0.31$$

$$\rho_{Ti} = 0.16 \text{ lb/in}^3$$

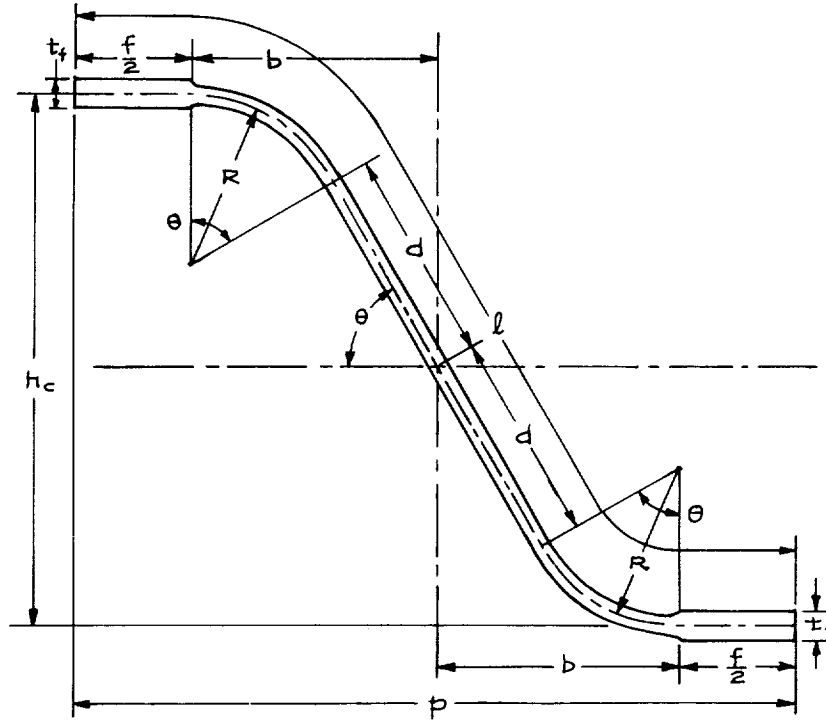


Figure 5. Corrugation leg of a truss core.

The effective elastic constants used for the titanium honeycomb cores are given in the following  
For case 1 core orientation

$$E_{cx} = 2.7778 \times 10^4 \text{ lb/in}^2$$

$$E_{cy} = 2.7778 \times 10^4 \text{ lb/in}^2$$

$$E_{cz} = 2.7778 \times 10^5 \text{ lb/in}^2$$

$$G_{cxy} = 0.00613 \text{ lb/in}^2$$

$$G_{cyz} = 0.81967 \times 10^5 \text{ lb/in}^2$$

$$G_{czx} = 1.81 \times 10^5 \text{ lb/in}^2$$

$$\nu_{cxy} = 0.658 \times 10^{-2}$$

$$\nu_{cyz} = 0.643 \times 10^{-6}$$

$$\nu_{czx} = 0.643 \times 10^{-6}$$

$$\rho_{HC} = 3.674 \times 10^{-3} \text{ lb/in}^3$$

For case 2 core orientation: subscripts  $x$  and  $y$  are interchanged.

## 6.2 Convergency of Eigenvalue Solutions

To find the minimum number of simultaneous equations (written out from eq. (30)) required to yield sufficiently accurate eigenvalue solutions, the order of determinants (eq. (32) and (33)) was gradually increased from order 4

until the eigenvalues sufficiently converged. Figure 6, which is the plots of table 1, shows the convergency behavior of  $k_{xy}$  (even and odd) with the increase of the order of matrices for a special case of  $k_x = 0$  and  $\frac{c}{a} = 1$ , for truss-core sandwich panel of case 1 core orientation.

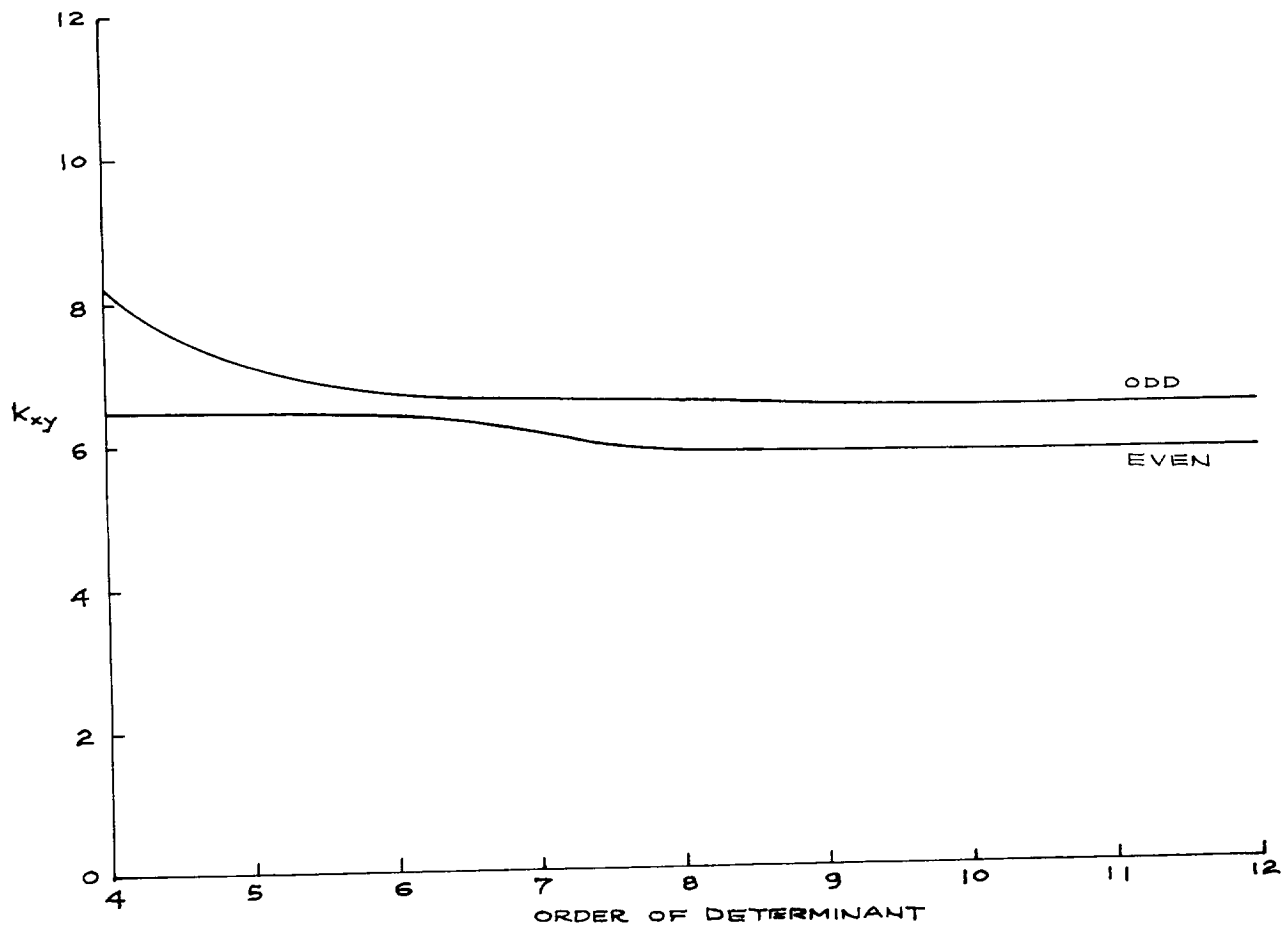


Figure 6. Convergency of shear buckling solutions with an increase of the order of matrix.  $k_x = 0$ ,  $\frac{c}{a} = 1$ .

Table 1. Convergency of  $k_{xy}$  for truss-core sandwich panel of case 1 core orientation.

Order of determinant	$k_{xy}$ , even	$k_{xy}$ , odd
4	6.43	8.19
6	6.39	6.64
8	5.79	6.58
10	5.76	6.34
12	5.72	6.33

The values of  $k_{xy}$  (even and odd) have sufficiently converged at order 12. Thus, in the actual calculations of  $k_{xy}$  for any given values of  $k_x$  and  $\frac{c}{a}$ , the order of matrices was set to be 12 (eq. (32) and (33)).

### 6.3 Buckling Interaction Curves

Figures 7 through 10 show buckling interaction curves for the truss-core and honeycomb-core sandwich panels of the same specific weight and of different core orientations, respectively. Both symmetric and antisymmetric buckling cases are shown for different aspect ratios of the panels. For the square panels ( $\frac{c}{a} = 1$ ), the antisymmetric buckling interaction curves (broken curves) lay on the right hand side of the symmetric buckling interaction curves without intersecting. For  $\frac{c}{a} \geq 2$ , the symmetric and antisymmetric curves intersect at certain combined loading points at the shear dominated combined loading region. Figure 11 shows the comparison of the composite buckling interaction curves for the two types of sandwich panels. Those composite buckling interaction curves were constructed from figures 7 through 10 by combining portions of symmetric and antisymmetric buckling interaction curves to give minimum combined buckling loads. For square panels ( $\frac{c}{a} = 1$ ) (any type), the core orientation has no effect on the pure compressive and pure shear buckling strength of the panels, and has negligible effect on the combined-load buckling strength of the panels. When the aspect ratio is increased, the effect of core orientation becomes conspicuous. For square panels ( $\frac{c}{a} = 1$ ), the truss-core sandwich panels (any core orientation) have higher buckling strength than the honeycomb-core sandwich panels (any core orientation) when the loading is compression dominated combined loading. When the loading is shear dominated, the latter has the higher buckling strength. For an aspect ratio greater than 1, the two cases of interaction curves of honeycomb-core sandwich panel practically lay between the two interaction curves for the truss-core sandwich panel. Figure 12 shows  $k_x$  plotted as a function of  $\frac{c}{a}$  for the two types of sandwich panels.

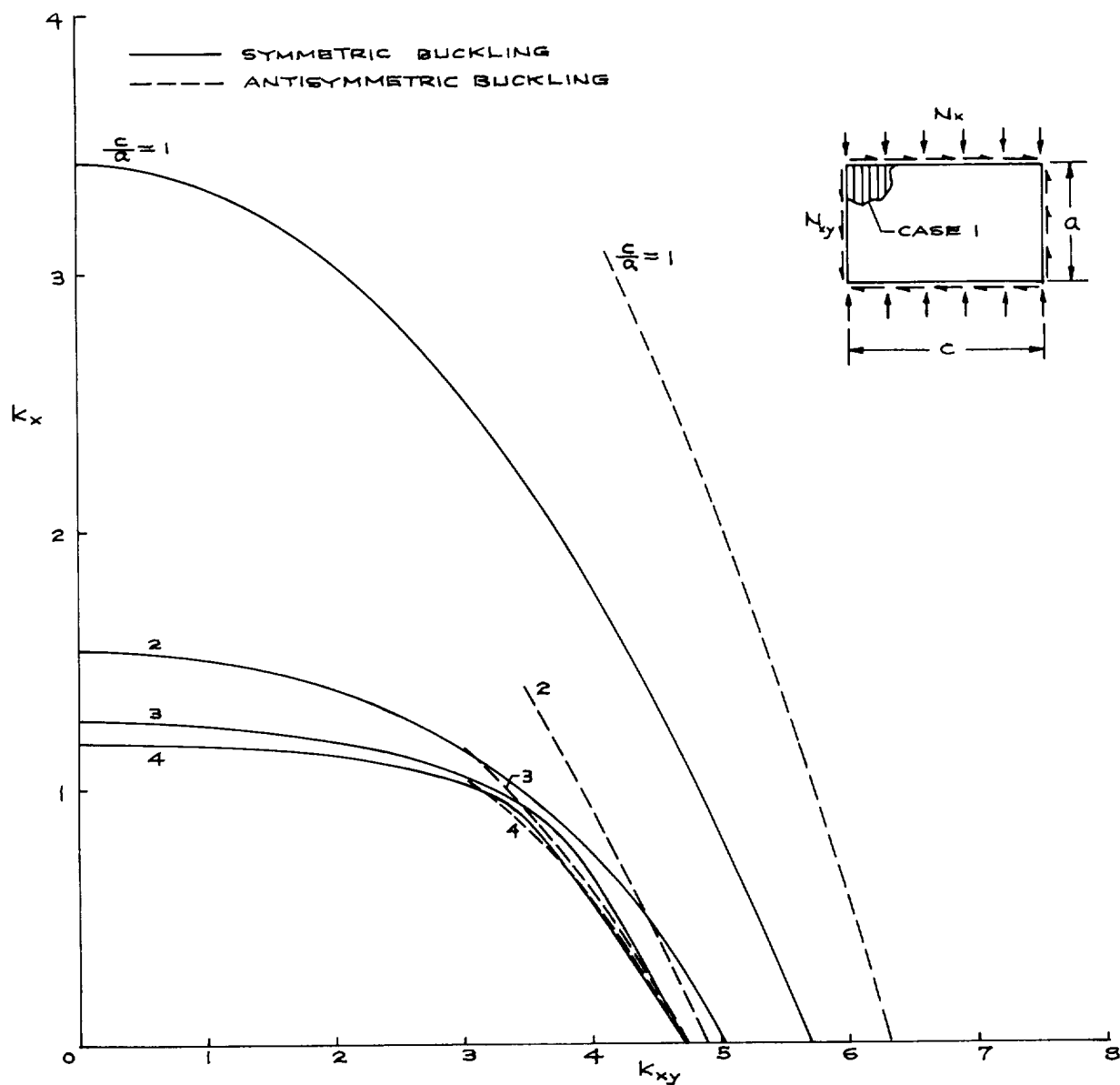


Figure 7. Buckling interaction plots for truss-core sandwich panels of different aspect ratios.  $N_x$  is parallel to the corrugation axis.

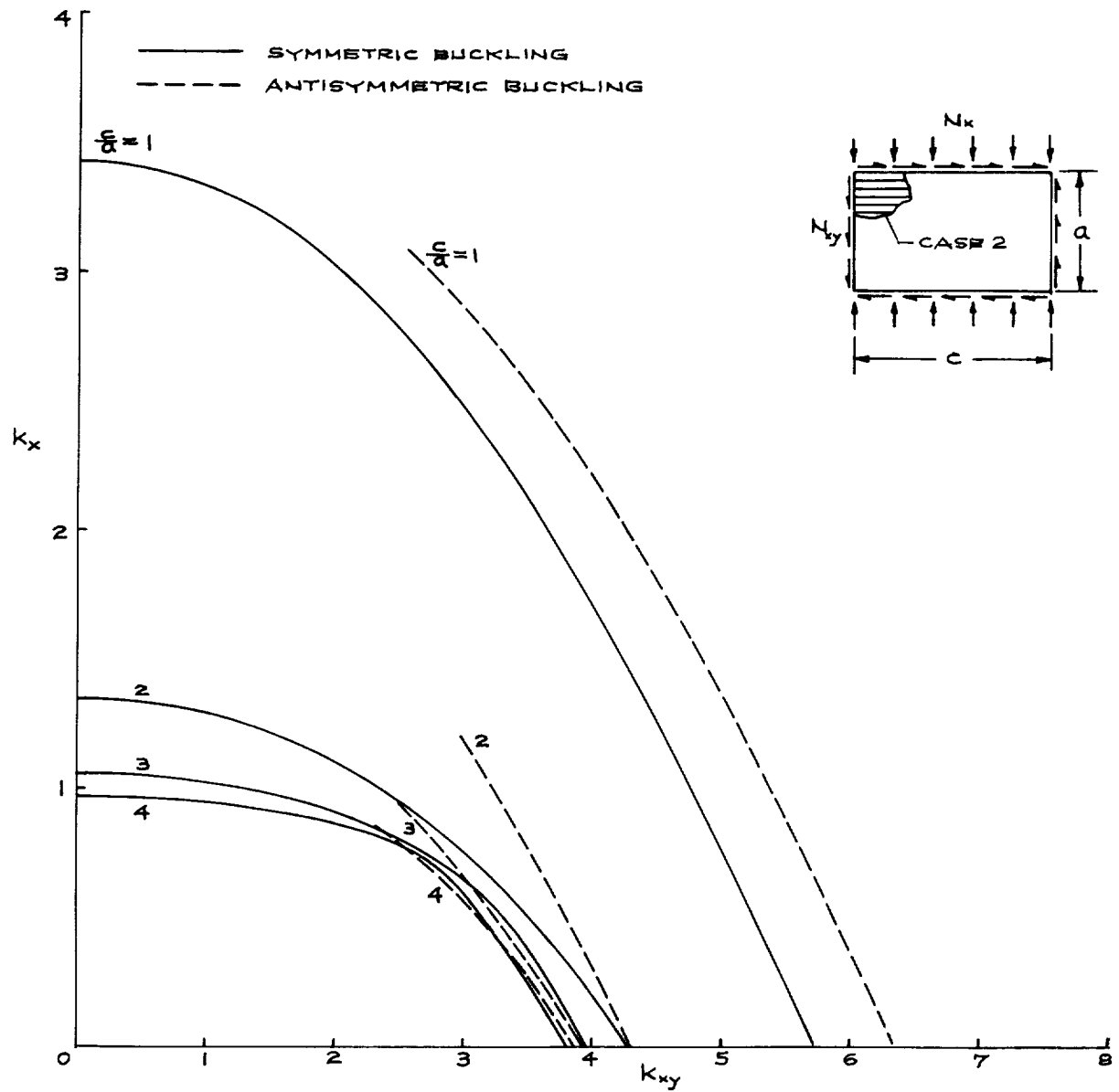


Figure 8. Buckling interaction plots for truss-core sandwich panels of different aspect ratios.  $N_x$  is perpendicular to the corrugation axis.

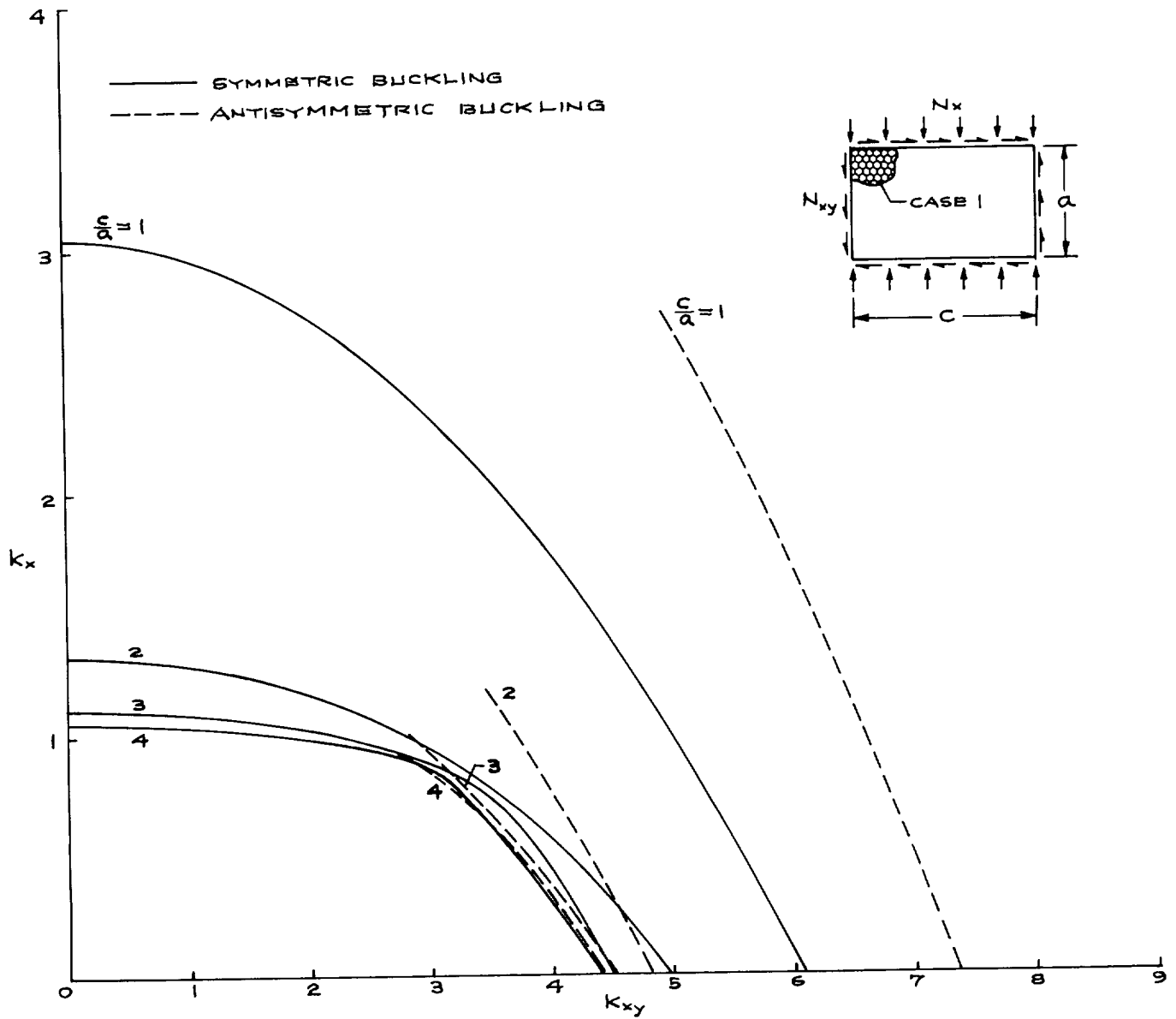


Figure 9. Buckling interaction plots for honeycomb-core sandwich panels of different aspect ratios. Case 1 core orientation.

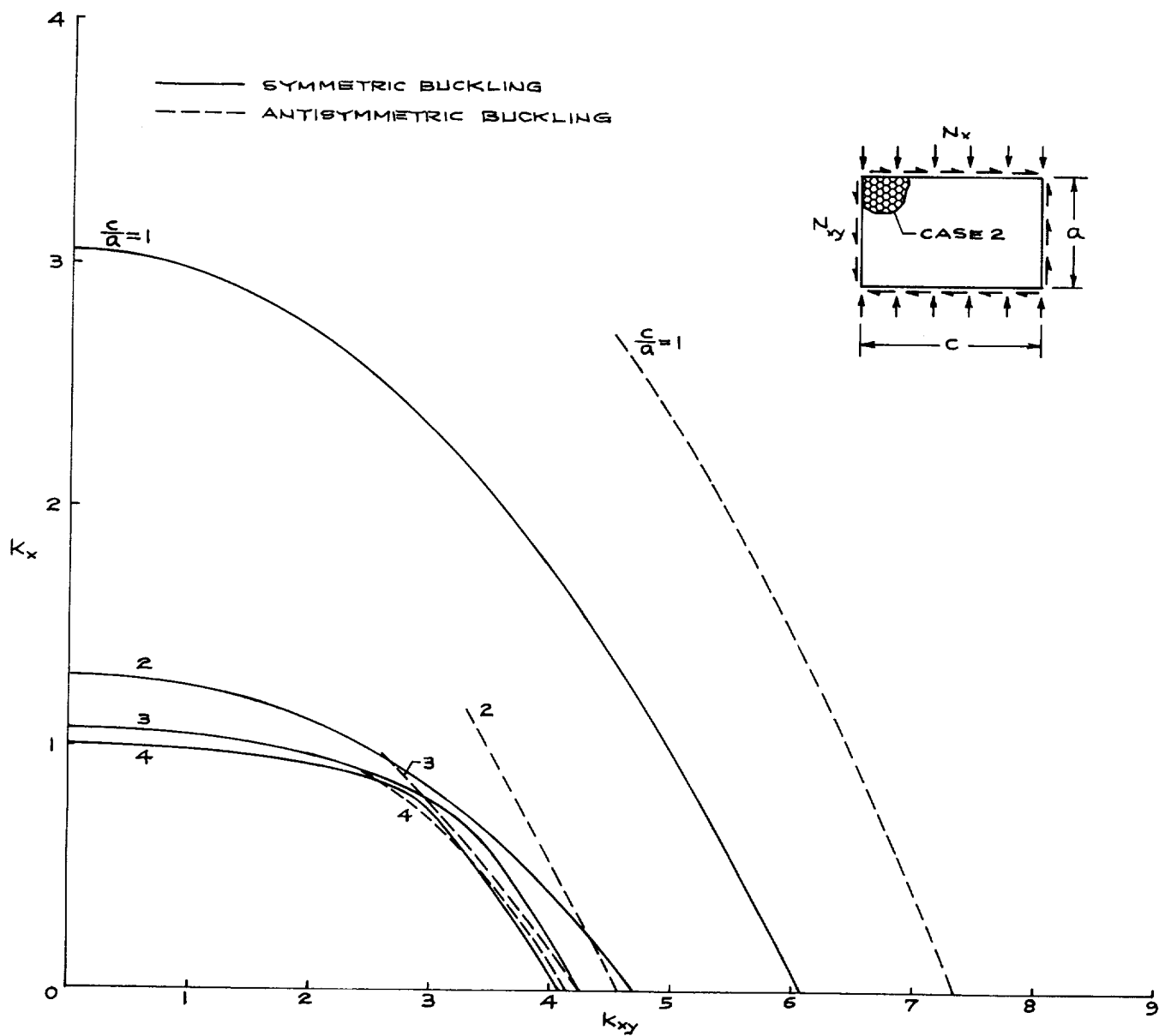


Figure 10. Buckling interaction plots for honeycomb-core sandwich panels of different aspect ratios. Case 2 core orientation.



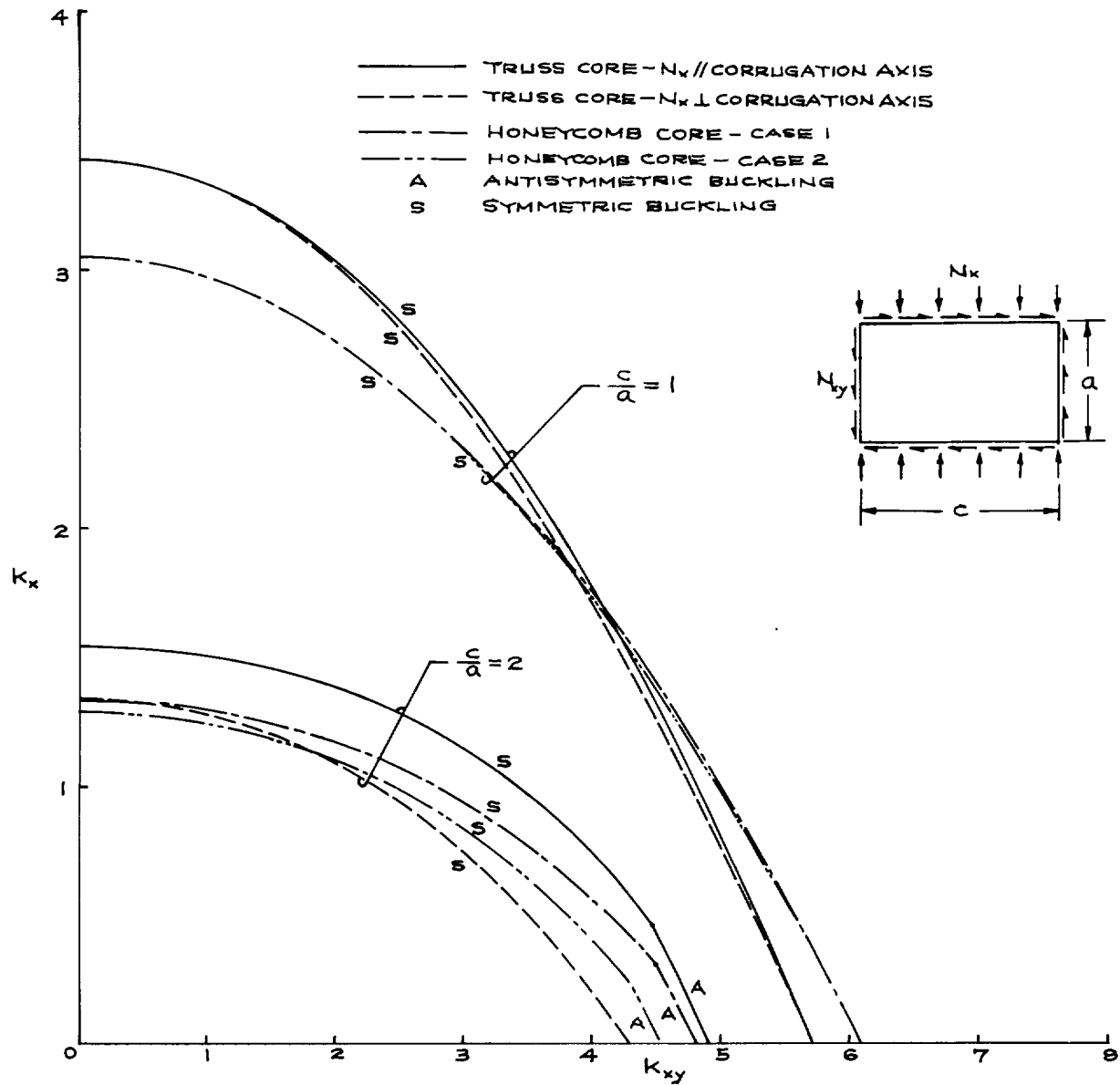


Figure 11(a). Comparison of buckling strength of truss-core and honeycomb-core sandwich panels having the same specific weight.

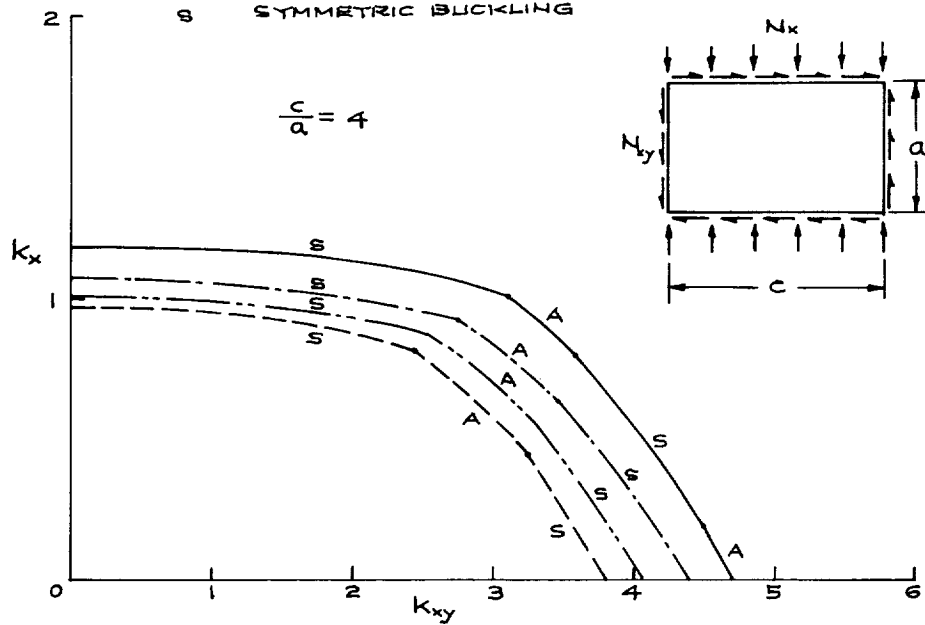
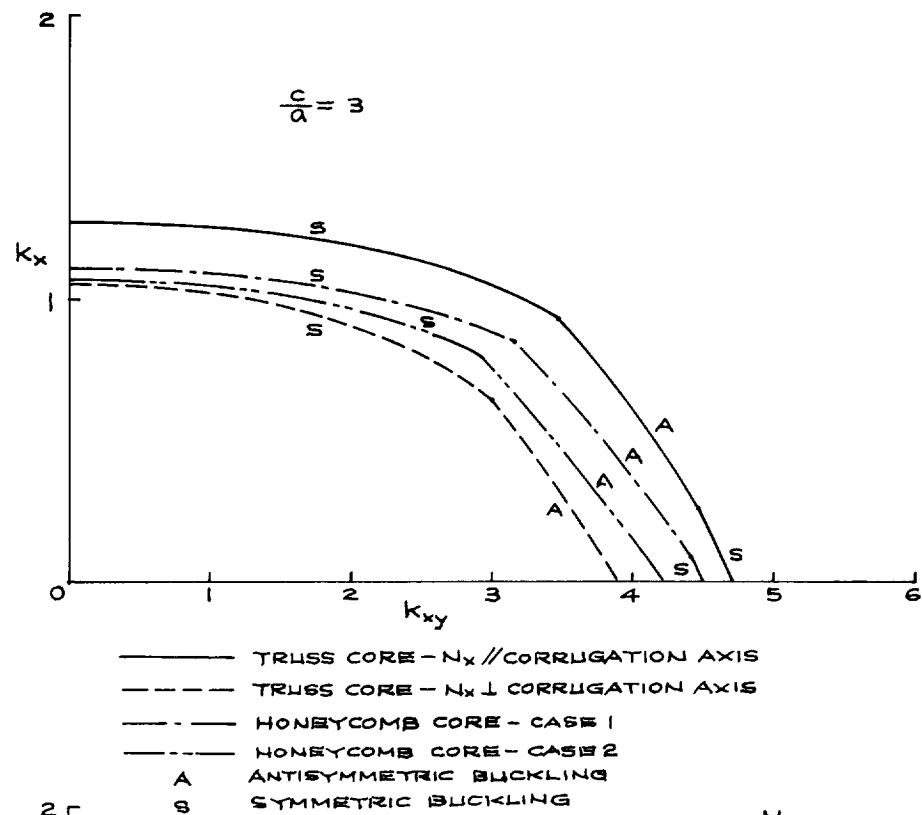


Figure 11(b). Concluded.

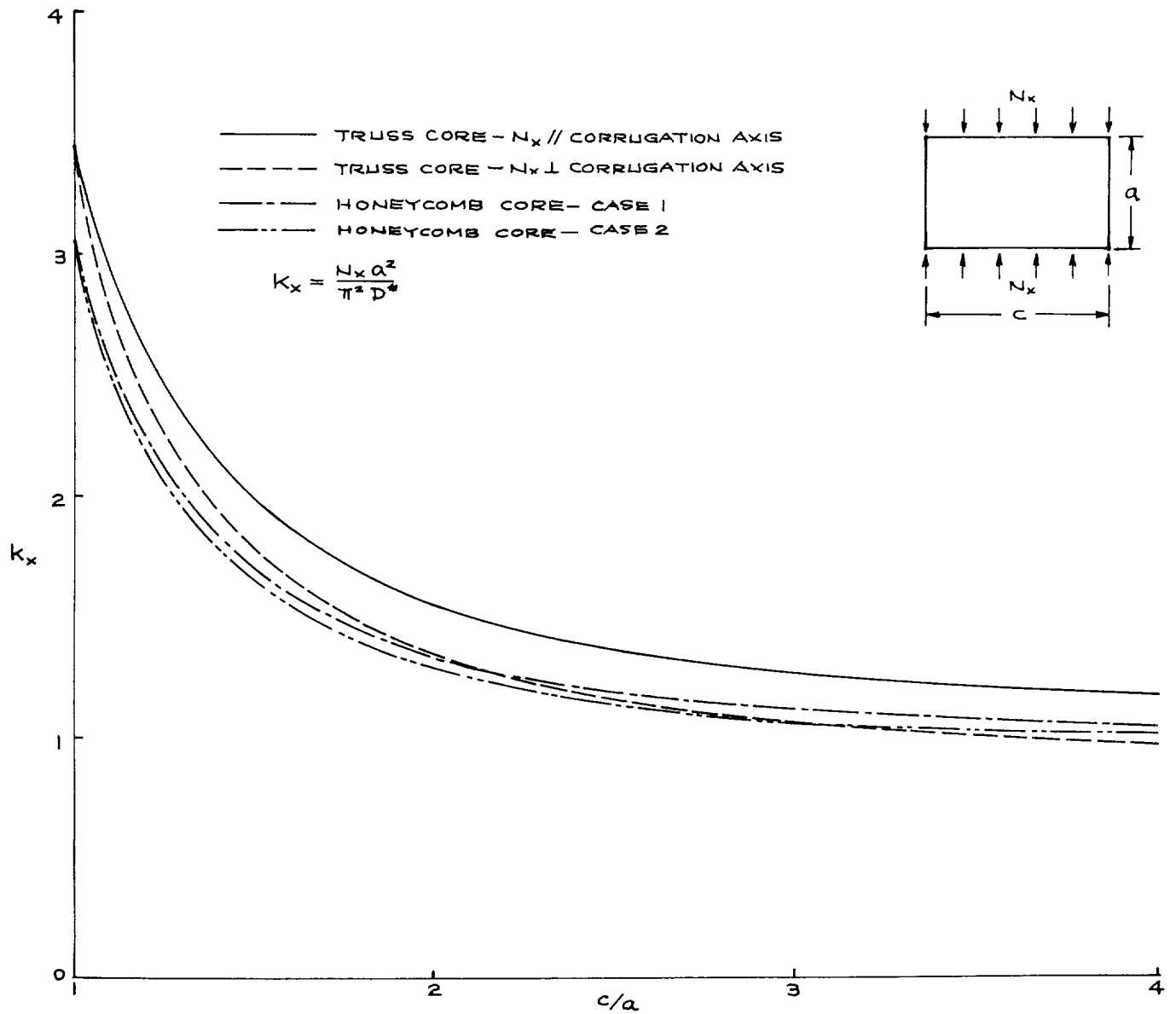


Figure 12. Comparison of compressive buckling strength of truss-core and honeycomb-core sandwich panels having the same specific weight.

It is seen that the value of  $k_x$  decreases sharply as the aspect ratio  $\frac{c}{a}$  is increased from  $\frac{c}{a} = 1$  to  $\frac{c}{a} = 2$ . Beyond  $\frac{c}{a} = 2$ , the rate of decrease of  $k_x$  with the increase in  $\frac{c}{a}$  becomes less severe. For compressive buckling strength, the truss-core sandwich panel of case 1 core orientation has a higher value of  $k_x$  than the honeycomb-core sandwich panel for all the range of panel aspect ratio  $\frac{c}{a}$ . For case 2 core orientation, the former has a higher value of  $k_x$  than the latter only up to  $\frac{c}{a} \approx 2.1$ . Figure 13 shows similar plots for  $k_{xy}$ . The rate of decrease of  $k_{xy}$  with the increase in  $\frac{c}{a}$  is less severe as compared with the compressive buckling case (fig. 12). The honeycomb-core sandwich panel has higher shear buckling strength only in the range of aspect ratio  $1 < \frac{c}{a} < 1.5$  (case 1 core orientation) or  $1 < \frac{c}{a} < 1.25$  (case 2 core orientation). Beyond  $\frac{c}{a} = 1.5$ , the truss-core sandwich panel with case 1 core orientation has higher shear buckling strength. Table 2 summarizes the values of  $k_x$  and  $k_{xy}$  for different panel aspect ratios.

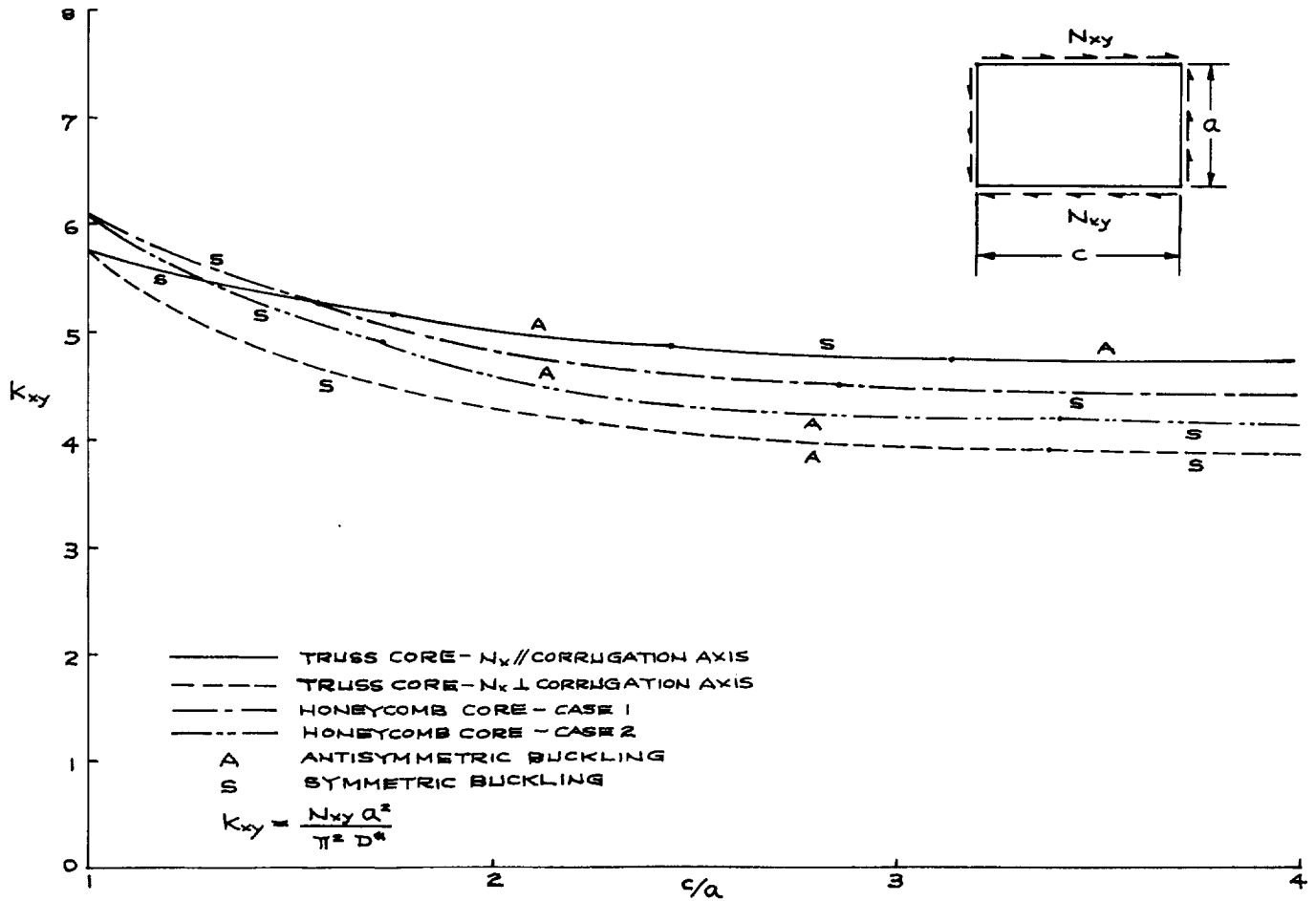


Figure 13. Comparison of shear buckling strength of truss-core and honeycomb-core sandwich panels having the same specific weight.

Table 2. Buckling load factors for truss-core and honeycomb-core sandwich panels having same specific weight.

$\frac{c}{a}$	$k_x$				$k_{xy}$ (symmetric)				$k_{zy}$ (antisymmetric)			
	Truss-core sandwich panel		Honeycomb-core sandwich panel		Truss-core sandwich panel		Honeycomb-core sandwich panel		Truss-core sandwich panel		Honeycomb-core sandwich panel	
	case 1	case 2	case 1	case 2	case 1	case 2	case 1	case 2	case 1	case 2	case 1	case 2
1	3.4321	3.4321	3.0529	3.0529	5.7160	5.7160	6.0831	6.0834	6.3284	6.3284	7.3575	7.3575
2	1.5533	1.3450	1.3351	1.2943	5.0279	4.2812	4.9674	4.6761	4.9106	4.3001	4.8060	4.5747
3	1.2724	1.0620	1.1177	1.0788	4.7186	3.9598	4.5042	4.2364	4.7496	3.9186	4.5115	4.2163
4	1.1799	0.9709	1.0495	1.0117	4.7497	3.8200	4.4070	4.0988	4.7148	3.8605	4.4279	4.1417

Figures 14 through 17 show the buckling interaction curves plotted in the stress-ratio spaces for the truss-core and honeycomb-core sandwich panels of different core orientations, respectively. For the aspect ratios  $\frac{c}{a} = 1, 2$ , the buckling interaction curves for the two types of panels are continuous curves. However, for  $\frac{c}{a} = 3, 4$ , the buckling interaction curves in figures 14 through 17 are discontinuous composite curves constructed from symmetric and antisymmetric buckling interaction curves. Those buckling interaction curves in the stress-ratio space for the two types of sandwich panels may be described by the following mathematical equations shown in table 3.

Table 3. Equations for describing buckling interaction curves in stress-ratio space.

$\frac{c}{a}$	Truss-core sandwich panel		Honeycomb-core sandwich panel	
	case 1	case 2	case 1	case 2
1	$R_x + R_{xy}^{2.04} \approx 1$	$R_x + R_{xy}^{1.92} \approx 1$	$R_x + R_{xy}^{2.00} \approx 1$	$R_x + R_{xy}^{1.98} \approx 1$
2	$R_x + R_{xy}^{2.86} \approx 1$	$R_x + R_{xy}^{2.29} \approx 1$	$R_x + R_{xy}^{2.52} \approx 1$	$R_x + R_{xy}^{2.39} \approx 1$
3	Discontinuous curve	Discontinuous curve	Discontinuous curve	Discontinuous curve
4	Discontinuous curve	Discontinuous curve	Discontinuous curve	Discontinuous curve

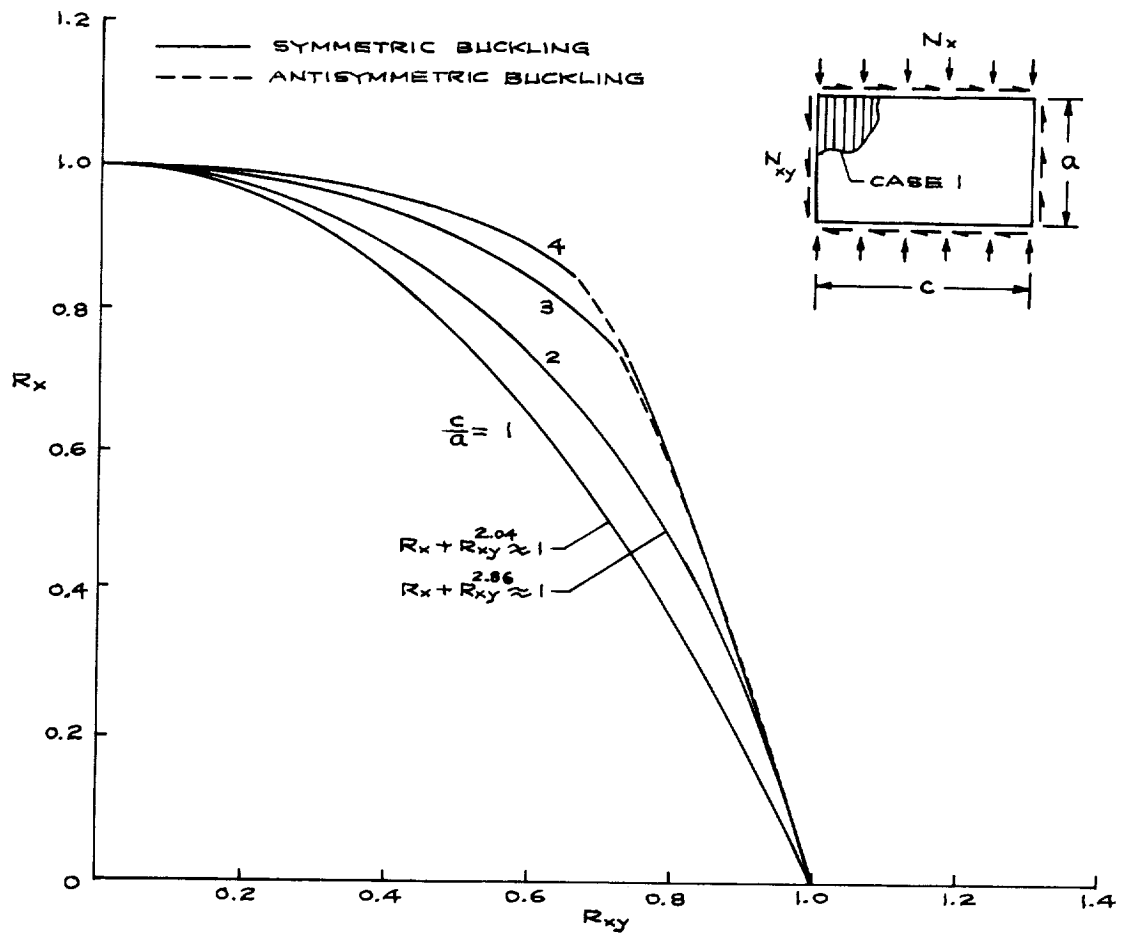


Figure 14. Buckling interaction plots in stress ratio space for truss-core sandwich panels of different aspect ratios.  $N_x$  is parallel to the corrugation axis.

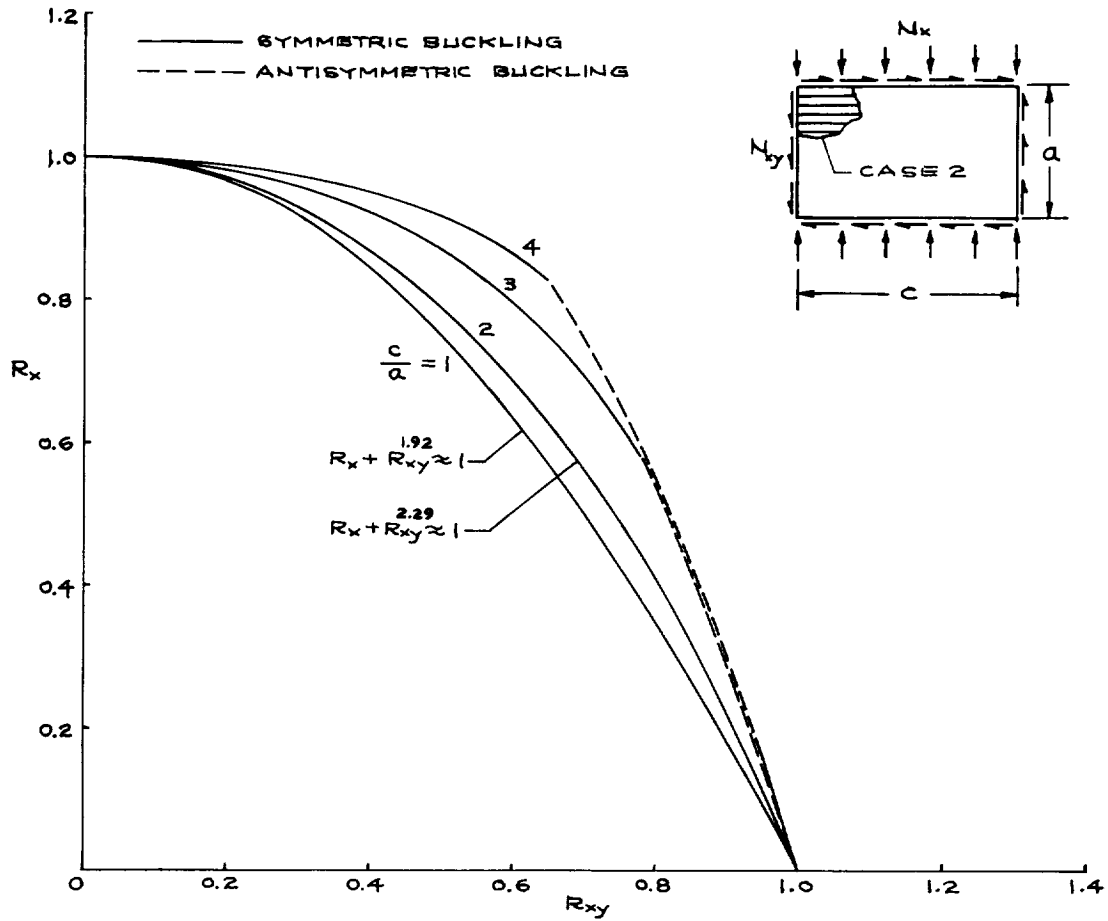


Figure 15. Buckling interaction plots in stress ratio space for truss-core sandwich panels of different aspect ratios.  $N_x$  is perpendicular to the corrugation axis.

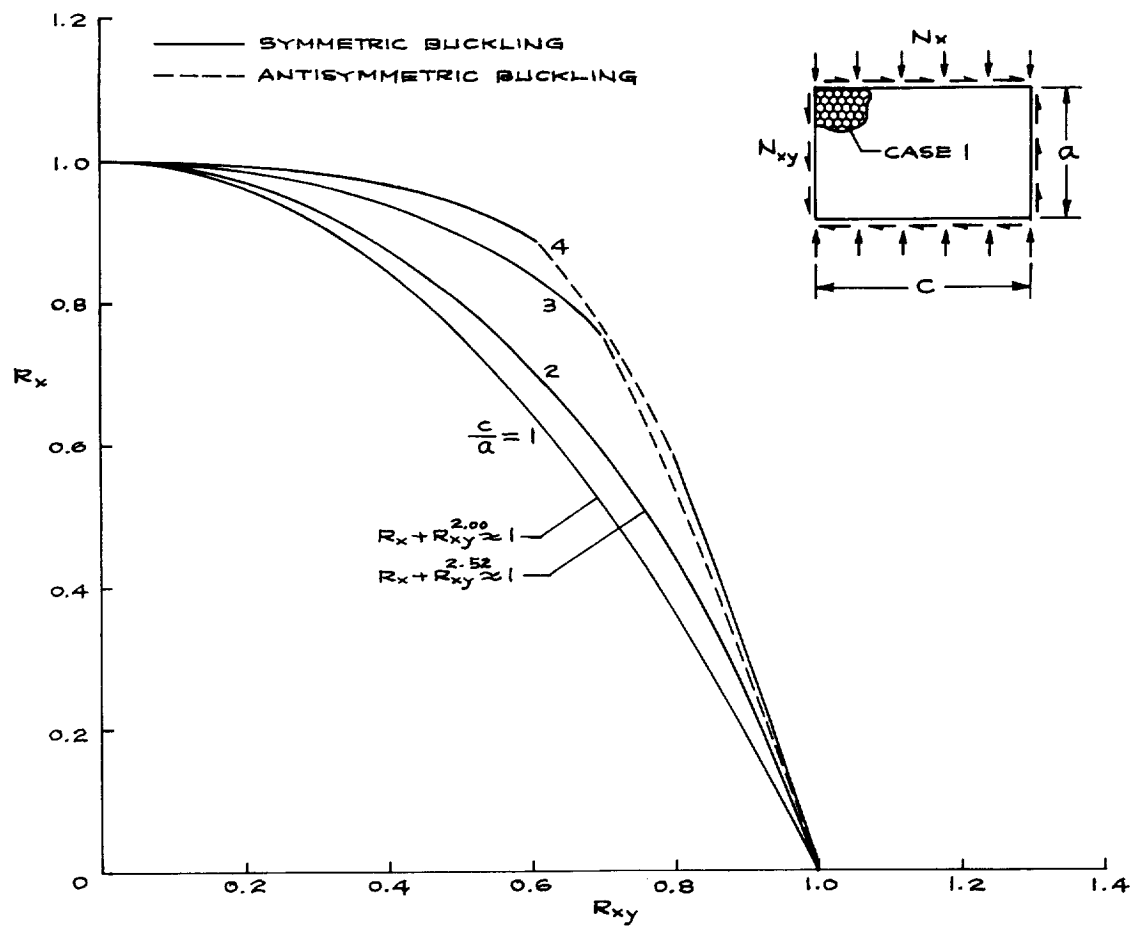


Figure 16. Buckling interaction plots in stress ratio space for honeycomb-core sandwich panels of different aspect ratios. Case 1 core orientation.



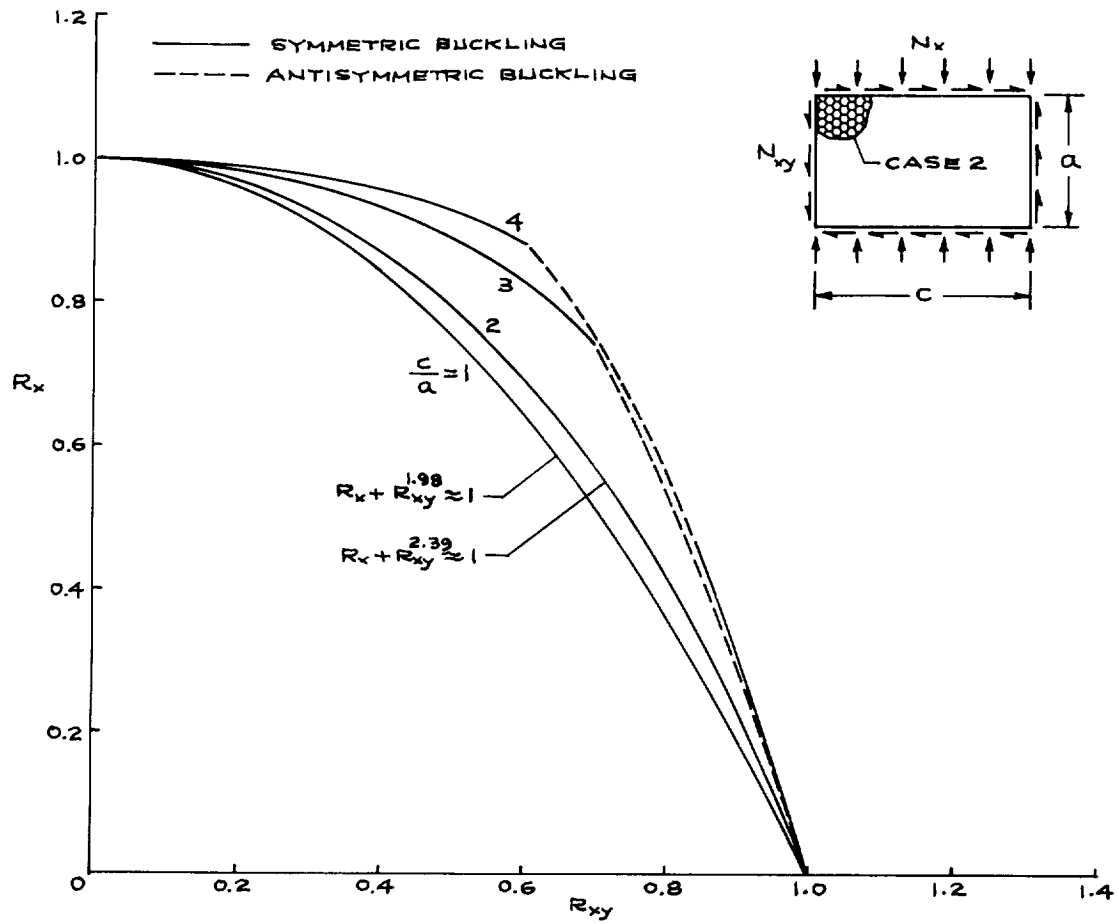


Figure 17. Buckling interaction plots in stress ratio space for honeycomb-core sandwich panels of different aspect ratios. Case 2 core orientation.

## 7 CONCLUDING REMARKS

Combined-load buckling analysis was performed on the truss-core and honeycomb-core sandwich panels having the same specific weight, and the combined-load buckling interaction curves were generated for these two types of sandwich panels with different panel aspect ratios and different core orientations. The results of the analysis are summarized in the following

1. The infinite number of simultaneous characteristic equations for calculating the shear buckling load components could be cut off at 12 (i.e., order of matrix 12) to yield sufficiently accurate eigenvalue solutions for shear buckling loads.
2. For square sandwich panels of both types, only the symmetric buckling will take place. For a panel aspect ratio greater than one, both symmetric and antisymmetric bucklings will take place. The antisymmetric buckling will occur when the combined loading is shear dominated.
3. The buckling interaction curves in the stress ratio space for both types of sandwich panels are continuous curves for low-panel aspect ratios, but become discontinuous composite curves at higher panel aspect ratios.
4. The square-shaped sandwich panel (any type) has the highest combined-load buckling strength, and the combined-load buckling strength decreases sharply as the panel aspect ratio is increased.
5. For a square sandwich panel (any type) the core orientation has no effect on pure compressive and pure shear buckling strength, but has negligible effect on the combined-load buckling strength. When the panel aspect ratio is increased, the effect of core orientation on the combined-load buckling strength becomes conspicuous.
6. For square sandwich panels, the truss-core sandwich panels (two core orientations) have higher buckling strength than the honeycomb-core sandwich panels (two core orientations) when the combined loading is compression dominated. The reverse is true when the combined loading is shear dominated.
7. For an aspect ratio greater than one, the two buckling interaction curves of honeycomb-core sandwich panels of two core orientations practically lay between the two buckling interaction curves of truss-core sandwich panels of two core orientations.

## APPENDIX

### FLEXURAL, TWISTING, AND TRANSVERSE SHEAR STIFFNESSES

The flexural stiffnesses  $D_x$  and  $D_y$ , the twisting stiffness  $D_{xy}$ , and the transverse shear stiffnesses  $D_{Qx}$  and  $D_{Qy}$  of the truss-core and honeycomb-core sandwich panels are written in the following for anisotropic face sheet material and isotropic core material.

Truss-core sandwich panel, case 1 core orientation

$$D_x = E_x I_s + E_c \bar{I}_c \quad (\text{A-1})$$

$$D_y = E_y I_s \frac{1 + \frac{E_c \bar{I}_c}{E_y I_s}}{1 + (1 - \nu_{xy} \nu_{yx}) \frac{E_c \bar{I}_c}{E_y I_s}} \quad (\text{A-2})$$

$$D_{xy} = 2 G_{xy} I_s \quad (\text{A-3})$$

$$D_{Qx} = \frac{G_c t_c h^2}{p \ell} \quad (\text{A-4})$$

$$D_{Qy} = \bar{S} h \frac{E_c}{1 - \nu_c^2} \left( \frac{t_c}{h_c} \right)^3 \quad (\text{A-5})$$

In the above equations,  $\{E_x, E_y, G_{xy}, \nu_{xy}, \nu_{yx}\}$  and  $\{E_c, G_c, \nu_c\}$  are the elastic constants associated, respectively, with the anisotropic face sheet material and the isotropic truss-core material,  $h$  is the depth of the sandwich panel,  $p$  is one half of the corrugation pitch,  $t_s$  is the thickness of the upper and lower face sheets,  $t_c$  is the final thickness of the core sheet after superplastic expansion and is related to the original core sheet thickness  $t_f$  through (figs. 1, 5)

$$t_c = t_f \frac{p-f}{\ell-f} \xrightarrow{f=0} t_f \cos \theta \quad (\text{A-6})$$

where  $f$  is the length of corrugation leg horizontal flat segment,  $\theta$  is the corrugation angle, and  $h_c$  in equation (A-5) is the depth of the corrugation defined as

$$h_c = h - (t_s + t_f) \quad (\text{A-7})$$

and finally,  $\ell$  is the length of corrugation leg expressed as

$$\ell = f + 2(d + R\theta) \quad (\text{A-8})$$

where  $d$  is one half the length of the corrugation leg diagonal segment, and  $R$  is the radius of the circular arc segments of the corrugation leg (fig. 5).

In equations (A-1) and (A-2),  $I_s$  is the moment of inertia of the face sheets taken with respect to the centroidal axis of the sandwich panel, and  $\bar{I}_c$  is the moment of inertia of the corrugation leg taken with respect to the corrugation core centroidal axis (parallel to  $y$  axis). The expressions for  $I_s$  and  $\bar{I}_c$  are given in the following

$$I_s = \frac{1}{2} t_s h^2 + \frac{1}{6} t_s^3 \quad (\text{A-9})$$

$$\begin{aligned} \bar{I}_c = \frac{h_c^3 t_c}{p} \left\{ \frac{1}{4} \frac{f}{h_c} \frac{t_f}{t_c} \left( 1 + \frac{1}{3} \frac{t_c^2}{h_c^2} \right) + \frac{2}{3} \frac{d^3}{h_c^3} \left( \sin^2 \theta + \frac{1}{4} \frac{t_c^2}{d^2} \cos^2 \theta \right) \right. \\ \left. + \frac{R}{h_c} \left[ \frac{\theta}{2} - \frac{R^2}{h_c^2} \sin \theta (1 - \cos \theta) - \frac{R}{h_c} \left( 2 - 3 \frac{R}{h_c} \right) (\theta - \sin \theta) \right] \right\} \quad (\text{A-10}) \end{aligned}$$

The nondimensional shear stiffness coefficient  $\bar{S}$  appearing in equation (A-5) is defined as (refs. 13, 19)

$$\bar{S} = \frac{6 \frac{h_c}{p} D_z^F t_c + \left(\frac{p}{h_c}\right)^2}{12 \left\{ \frac{h}{h_c} \frac{p}{h_c} D_z^F - 2 \left(\frac{p}{h_c}\right)^2 D_z^H + \frac{h_c}{h} \left[ 6 \frac{t_c}{h} \left( D_z^F D_y^H - D_z^H^2 \right) + \left(\frac{p}{h_c}\right)^3 D_y^H \right] \right\}} \quad (\text{A-11})$$

where the nondimensional parameters  $D_z^F$ ,  $D_z^H$ , and  $D_y^H$  are defined as

$$\begin{aligned} D_z^F = & \frac{2}{3} \left( \frac{d}{h_c} \right)^3 \cos^2 \theta + \frac{2}{3} \frac{I_c}{I_f} \left[ \frac{1}{8} \left( \frac{p}{h_c} \right)^3 - \left( \frac{b}{h_c} \right)^3 \right] \\ & + \frac{R}{h_c} \left[ 2 \left( \frac{b}{h_c} \right)^2 \theta - 4 \frac{Rb}{h_c^2} (1 - \cos \theta) + \left( \frac{R}{h_c} \right)^2 (\theta - \sin \theta \cos \theta) \right] \\ & + \frac{I_c}{h_c^2 t_c} \left[ 2 \frac{d}{h_c} \sin^2 \theta + \frac{R}{h_c} (\theta - \sin \theta \cos \theta) \right] \end{aligned} \quad (\text{A-12})$$

$$\begin{aligned} D_y^H = & \frac{2}{3} \left( \frac{d}{h_c} \right)^3 \sin^2 \theta + \frac{1}{2} \left( \frac{R}{h_c} \theta + \frac{1}{2} \frac{f}{h_c} \frac{I_c}{I_f} \right) \\ & - \left( \frac{R}{h_c} \right)^2 \left[ \left( 2 - 3 \frac{R}{h_c} \right) (\theta - \sin \theta) + \frac{R}{h_c} \sin \theta (1 - \cos \theta) \right] \\ & + \frac{I_c}{h_c^2 t_c} \left[ \frac{f}{h_c} \frac{t_c}{t_f} + 2 \frac{d}{h_c} \cos^2 \theta + \frac{R}{h_c} (\theta + \sin \theta \cos \theta) \right] \end{aligned} \quad (\text{A-13})$$

$$\begin{aligned} D_z^H = & \frac{2}{3} \left( \frac{d}{h_c} \right)^3 \sin \theta \cos \theta + \frac{1}{2} \frac{I_c}{I_f} \left[ \frac{1}{4} \left( \frac{p}{h_c} \right)^2 - \left( \frac{b}{h_c} \right)^2 \right] \\ & + \frac{R}{h_c} \left\{ \frac{b}{h_c} \theta - 2 \frac{Rb}{h_c^2} (\theta - \sin \theta) - \frac{R}{h_c} (1 - \cos \theta) \left[ 1 - \frac{R}{h_c} (1 - \cos \theta) \right] \right\} \\ & - \frac{I_c}{h_c^2 t_c} \left( 2 \frac{d}{h_c} \sin \theta \cos \theta + \frac{R}{h_c} \sin^2 \theta \right) \end{aligned} \quad (\text{A-14})$$

where  $b(= \frac{1}{2}(p - f))$  is one half of the horizontal projected length of the nonhorizontal region of the corrugation leg (fig. 5), and the moments of inertia  $I_f$  and  $I_c$  of the flat and diagonal regions of the corrugation leg are defined respectively as

$$I_f = \frac{1}{12} t_f^3, \quad I_c = \frac{1}{12} t_c^3 \quad (\text{A-15})$$

In case 2 core orientation, subscripts  $x$  and  $y$  in equations (A-1) through (A-5) are interchanged.

Honeycomb-core sandwich, case 1 core orientation

$$D_x = E_x I_s \quad (\text{A-16})$$

$$D_y = E_y I_s \quad (\text{A-17})$$

$$D_{xy} = 2 G_{xy} I_s \quad (\text{A-18})$$

$$D_{Qx} = G_{cxz} h'_c \quad (\text{A-19})$$

$$D_{Qy} = G_{cyz} h'_c \quad (\text{A-20})$$

where  $h'_c$  is the honeycomb-core depth (fig. 2) defined as

$$h'_c = h - t_s \quad (\text{A-21})$$

In case 2 core orientation, subscripts  $x$  and  $y$  in equations (A-16) through (A-20) are interchanged.

## REFERENCES

1. Plank, P.P., I.F. Sakata, G.W. Davis, and C.C. Richie, *Hypersonic Cruise Vehicle Wing Structure Evaluation*, NASA CR-1568, 1970.
2. Greene, Bruce E., *Substantiation Data for Advanced Beaded and Tubular Structural Panels-Volume 1, Design and Analysis*, NASA CR-132460, 1974.
3. Musgrove, Max D., and Russell F. Northrop, *Substantiation Data for Advanced Beaded and Tubular Structural Panels-Volume 2, Fabrication*, NASA CR-132482, 1974.
4. Hedges, Philip C., and Bruce E. Greene, *Substantiation Data for Advanced Beaded and Tubular Structural Panels-Volume 3, Testing*, NASA CR-132515, 1974.
5. Musgrove, Max D., and Bruce E. Greene, *Advanced Beaded and Tubular Structural Panels*, NASA CR-2514, 1975.
6. Greene, Bruce E., and Russell F. Northrop, *Design and Fabrication of René 41 Advanced Structural Panels*, NASA CR-132646, 1975.
7. Musgrove, Max D., Bruce E. Greene, John L. Shideler, and Herman L. Bohon, "Advanced Beaded and Tubular Structural Panels," *J. Aircraft*, vol. 11, no. 2, Feb. 1974, pp. 68-75.
8. Shideler, John L., Herman L. Bohon, and Bruce E. Greene, "Evaluation of Bead-Stiffened Metal Panels," AIAA Paper No. 75-815, May 1975.
9. Siegel, William H., *Experimental and Finite Element Investigation of the Buckling Characteristics of a Beaded Skin Panel for a Hypersonic Aircraft*, NASA CR-144863, 1978.
10. Shideler, John L., Roger A. Fields, and Lawrence F. Reardon, *Tests of Beaded and Tubular Structural Panels, Recent Advances in Structures for Hypersonic Flight*, NASA CP-2065, Part II, 1978, pp. 539-576.
11. Ko, William L., John L. Shideler, and Roger A. Fields, *Buckling Characteristics of Hypersonic Aircraft Wing Tubular Panels*, NASA TM-87756, 1986.
12. Tenney, Darrel R., W. Barry Lisagor, and Sidney C. Dixon, "Materials and Structures for Hypersonic Vehicles," *J. Aircraft*, vol. 26, no. 11, Nov. 1989, pp. 953-970.
13. Ko, William L., "Elastic Stability of Superplastically Formed/Diffusion-Bonded Orthogonally Corrugated Core Sandwich Plates," AIAA Paper No. 80-0683, May 1980.

14. Ko, William L., *Comparison of Structural Behavior of Superplastically Formed/Diffusion-Bonded Sandwich Structures and Honeycomb Core Sandwich Structures*, NASA TM-81348, 1980.
15. Libove, Charles, and S.B. Batdorf, *A General Small-Deflection Theory for Flat Sandwich Plates*, NACA TN-1526, 1948.
16. Bert, Charles W., and K.N. Cho, "Uniaxial Compressive and Shear Buckling in Orthotropic Sandwich Plates by Improved Theory," AIAA Paper No. 86-0977, May 1986.
17. Batdorf, S.B., and Manuel Stein, *Critical Combinations of Shear and Direct Stress for Simply Supported Rectangular Flat Plates*, NACA TN-1223, 1947.
18. Stein, Manuel, and John Neff, *Buckling Stresses of Simply Supported Rectangular Flat Plates in Shear*, NACA TN-1222, 1947.
19. Libove, Charles, and Ralph E. Hubka, *Elastic Constants for Corrugated-Core Sandwich Plates*, NACA TN-2289, 1951.





1. Report No. NASA TM-4290		2. Government Accession No.		3. Recipient's Catalog No.	
4. Title and Subtitle  Combined Compressive and Shear Buckling Analysis of Hypersonic Aircraft Structural Sandwich Panels				5. Report Date May 1991	
				6. Performing Organization Code	
7. Author(s)  William L. Ko and Raymond H. Jackson				8. Performing Organization Report No. H-1694	
				10. Work Unit No. RTOP 532-09-01	
9. Performing Organization Name and Address NASA Dryden Flight Research Facility P.O. Box 273 Edwards, California 93523-0273				11. Contract or Grant No.	
				13. Type of Report and Period Covered Technical Memorandum	
12. Sponsoring Agency Name and Address  National Aeronautics and Space Administration Washington, DC 20546-3191				14. Sponsoring Agency Code	
15. Supplementary Notes					
16. Abstract  The combined-load (compression and shear) buckling equations were established for orthotropic sandwich panels by using the Rayleigh-Ritz method to minimize the panel total potential energy. The resulting combined-load buckling equations were used to generate buckling interaction curves for super-plastically-formed/diffusion-bonded titanium truss-core sandwich panels and titanium honeycomb-core sandwich panels having the same specific weight. The relative combined-load buckling strengths of these two types of sandwich panels are compared with consideration of their sandwich core orientations. For square and nearly square panels of both types, the combined load always induces symmetric buckling. As the panel aspect ratios increase, antisymmetric buckling will show up when the loading is shear-dominated combined loading. The square panel (either type) has the highest combined buckling strength, but the combined load buckling strength drops sharply as the panel aspect ratio increases. For square panels, the truss-core sandwich panel has higher compression-dominated combined-load buckling strength. However, for shear dominated loading, the square honeycomb-core sandwich panel has higher shear-dominated combined load buckling strength.					
17. Key Words (Suggested by Author(s)) Combined load buckling Honeycomb cores Sandwich panels Truss cores				18. Distribution Statement Unclassified — Unlimited  Subject category 39	
19. Security Classif. (of this report) Unclassified		20. Security Classif. (of this page) Unclassified		21. No. of Pages 36	
				22. Price A03	

